Noble gas insights into early impact delivery and volcanic outgassing to Earth's atmosphere: A limited role for the continental crust

Xinmu Zhang, Guillaume Avice, Rita Parai

Noble gas insights into early impact delivery and volcanic outgassing to Earth's atmosphere: a limited role for the continental crust

Xinmu J. Zhang[1,2*]†, Guillaume Avice[3], Rita Parai[1,2]

[1]Department of Earth and Planetary Sciences, Washington University in St. Louis, 1 Brookings Drive, St. Louis, MO, 63130 USA
[2]McDonnell Center for the Space Sciences, Washington University in St. Louis, 1 Brookings Drive, St. Louis, MO, 63130 USA
[3]Université Paris Cité, Institut de physique du globe de Paris, CNRS, F-75005 Paris, France
*corresponding author, email: xmjzhang@ucsd.edu
† now at Scripps Institution of Oceanography, UC San Diego

Keywords: noble gases; argon; neon; continental crust; mantle outgassing; volatile delivery

Abstract

Earth's atmosphere, crust and mantle have evolved together through continuous geochemical exchange throughout Earth's history. Constraints on the transport of volatile elements and compounds between these reservoirs are crucial for understanding how Earth could have stayed habitable for extended periods of time. Here we present a new forward model of He, Ne and Ar in the mantle, crust and atmosphere. We explore concentrations of noble gases at the end of accretion, bulk silicate Earth K/U ratios, crustal growth scenarios, and upper mantle processing rates throughout Earth's history. We search for parameter combinations that simultaneously satisfy observational constraints on present-day mantle $^{4}He/^{3}He$ and $^{40}Ar/^{36}Ar$ (sensitive to mantle outgassing and continental crust growth, which depletes the mantle of U, Th and K), atmospheric $^{20}Ne/^{22}Ne$ (which tracks the mix of outgassed vs. delivered Ne in the atmosphere), and atmospheric $^{40}Ar/^{36}Ar$ in the past and today (sensitive to volatile delivery, mantle outgassing and crustal growth). Leveraging this intertwined set of noble gas abundances and isotopic compositions yields new constraints on initial noble gas abundances in the mantle and on the proportions of atmospheric volatiles originating from delivery by impact degassing, mantle outgassing, and degassing of the continental crust. We find that atmospheric Ar isotopic evolution is primarily sensitive to the mantle processing rate history; the atmospheric Ar isotopic record should therefore not be used to reconstruct continental crust growth, but instead provides valuable insights into mantle processing rates. Our model predicts a measurably low $^{20}Ne/^{22}Ne$ ratio of ~9.7 in Archean atmospheric samples. Most of atmospheric primordial ^{36}Ar was directly delivered by chondritic bodies and not transferred to the atmosphere during an intense early episode of mantle outgassing. Nitrogen

41 delivered by impact degassing could account for the present-day atmospheric nitrogen inventory.

1. Introduction

Earth has experienced a vibrant planetary evolution since its accretion. The transport of volatiles (*e.g.*, water, carbon, nitrogen, and noble gases) between deep Earth and surface reservoirs is an important aspect of the coupled evolution of the mantle, continental crust and atmosphere. Improved constraints on volatile origins and the history of volatile exchange are crucial to our understanding of Earth's transformation into a habitable environment for living organisms.

Noble gases are powerful tracers of the coupled geochemical evolution of terrestrial reservoirs over time. The noble gases are chemically inert, are incompatible during partial melting, exhibit low solubilities in magma, and are isotopically sensitive to radioactive decay. Each noble gas element has at least one isotope that is produced by nuclear reactions, and at least one isotope that is primordial (*i.e.*, the nuclide is stable and not produced by any radioactive reactions). Each long-term geological process transporting volatile species among major geochemical reservoirs leaves an imprint on the isotopic composition of all of the noble gases and generates inherently linked geochemical signatures among the major terrestrial reservoirs. Therefore, isotopic systematics among multiple noble gas elements provide a rich record of the complex processes involved in the co-evolution of the mantle, the continental crust, and the atmosphere (*e.g.*, Allègre et al., 1987).

Helium (He) and argon (Ar) isotopes provide an example of how volatile origins and transport are recorded by noble gas systems in Earth reservoirs. ^{3}He is primordial, and ^{4}He is a radiogenic nuclide produced by α-decay of ^{238}U, ^{235}U and ^{232}Th. ^{36}Ar is a primordial nuclide and ^{40}Ar is produced from ^{40}K by electron capture. Noble gases and U, Th and K are incompatible during

63 partial melting, but the noble gases are largely degassed from melts to the atmosphere, generating
64 continuous fractionation of K/Ar and (U+Th)/He ratios in the solid Earth over time. As a mantle
65 reservoir is processed by partial melting, noble gases are transported from the mantle to the
66 atmosphere (called outgassing). Both primordial and radiogenic noble gas isotopes are lost from
67 the mantle, but only the radiogenic nuclides are subsequently produced by the decay of their
68 lithophile radioactive parent nuclides. Over time, outgassing leads to high radiogenic to primordial
69 noble gas isotopic ratios (*e.g.*, $^{4}He/^{3}He$ and $^{40}Ar/^{36}Ar$) in a mantle reservoir; the isotopic
70 composition of outgassed He and Ar supplied to the atmosphere evolves accordingly. Transport of
71 atmospheric gas into the mantle (called "regassing" hereafter) is not thought to be significant for
72 He, and its importance for mantle Ar is debated (Holland and Ballentine, 2006; Moreira and Raquin,
73 2007; Tucker et al., 2022; Péron and Mukhopadhyay, 2022). Thus, mantle and atmospheric
74 $^{4}He/^{3}He$ and $^{40}Ar/^{36}Ar$ ratios are time-integrated results reflecting continuous, long-term volatile
75 transport between the deep Earth and surface reservoirs.

76 He and Ar isotopes in mid-ocean ridge basalts (MORB) have long been used to generate
77 important constraints on mantle outgassing history (Ozima, 1975; Fisher, 1975; Sarda et al., 1985;
78 Moreira et al., 1998; Gonnermann and Mukhopadhyay, 2009). While strongly affected by mantle
79 outgassing, mantle $^{4}He/^{3}He$ and $^{40}Ar/^{36}Ar$ are also sensitive to growth of the continental crust,
80 which depletes the mantle of U, Th and K (*e.g.*, Allègre et al. 1983). A variety of studies have
81 modeled the growth of continental crust based on a combination of geophysical constraints (*e.g.*,
82 mantle thermal and convective evolution; Walzer and Hendel, 2017) and geochronology tools (*e.g.*,
83 U-Pb- and Hf-based zircon dating; Armstrong and Harmon, 1981; Belousova et al., 2010; Condie,

1998; Dhuime et al., 2012). The Ar isotopic composition of the atmosphere is closely tied to the evolution of the solid Earth (Ozima and Kudo, 1972; Sarda et al., 1985), and archives of atmospheric $^{40}Ar/^{36}Ar$ potentially provide another way to track continental crust growth (Hamano and Ozima, 1978; Pujol et al., 2013; Stuart et al., 2016; Guo and Korenaga, 2020).

Argon is the third-most abundant (0.93% by volume) gas in Earth's atmosphere, with a $^{40}Ar/^{36}Ar$ ratio of 298.56 ± 0.31 (Lee et al., 2006). The atmospheric $^{40}Ar/^{36}Ar$ ratio is orders of magnitude higher than an initial solar or chondritic $^{40}Ar/^{36}Ar$ ratio (Ott, 2002), reflecting outgassing of radiogenic ^{40}Ar from the solid Earth to the atmosphere. However, atmospheric $^{40}Ar/^{36}Ar$ is quite low compared to $^{40}Ar/^{36}Ar$ in the solid Earth: mantle $^{40}Ar/^{36}Ar$ is ~30,000 (Sarda et al., 1985; Moreira et al., 1998; Parai and Mukhopadhyay, 2021) and Ar in the continental crust should be largely ^{40}Ar. The canonical explanation for the relatively low ratio of $^{40}Ar/^{36}Ar$ in the present-day atmosphere compared to the mantle is a sudden, intense stage of gas loss ("catastrophic degassing") from the mantle (Fanale, 1971), early enough that radiogenic ^{40}Ar ingrowth had not yet strongly affected the mantle composition. Subsequent mantle outgassing models adopted a two-stage setup, with a brief catastrophic outgassing stage followed by a continuous outgassing stage after the end of accretion, with several orders of magnitude reduction in the outgassing rate between the two stages (Alexander and Ozima, 1978; Hamano and Ozima, 1978; Allègre et al., 1987; Fisher, 1975; Ozima, 1975; Sarda et al., 1985). Hamano and Ozima (1978) presented one such two-stage model tracing mantle Ar outgassing, K extraction from the mantle in the process of building the continental crust, and direct outgassing of the continental crust. The authors compared model results to a compilation of crustal ages to argue for continuous growth of the

105 continental crust rather than rapid early crustal formation.

106 The approach of applying Ar isotopic evolution models to constrain the growth of
107 continental crust has expanded as records of past atmospheric $^{40}Ar/^{36}Ar$ have been established.
108 Cadogan (1977) reported Ar isotopic compositions of ancient atmosphere trapped in Devonian-
109 aged Rhynie chert. Pujol et al. (2013) constrained the composition of the early atmosphere using
110 analyses of Archean hydrothermal quartz, and Avice et al. (2017) confirmed those results. Taking
111 into consideration how uncertainties in the age of the hydrothermal quartz (taken for example to
112 be 3.5 Ga, 3.0 Ga, or 2.7 Ga) would affect the inferred ancient atmospheric $^{40}Ar/^{36}Ar$ ratio, Pujol
113 et al. (2013) applied the two-stage outgassing model described in Hamano and Ozima (1978) and
114 argued for catastrophic early outgassing and limited continental crust growth (<10%) in the first
115 170 million years. Stuart et al. (2016) integrated high precision measurements of ancient
116 atmospheric Ar in the Rhynie chert to the model of Pujol et al. (2013) to further limit the extent of
117 Ar outgassing early in the continuous outgassing stage. In light of the high estimated proportion
118 of the present-day flux of ^{40}Ar from the solid Earth that comes from direct outgassing of the
119 continental crust (*e.g.,* Allègre et al., 1987; Bender et al., 2008), Stuart et al. argued for minimal
120 continental crust growth prior to 4 Ga. However, the integrated atmospheric ^{40}Ar contribution from
121 direct outgassing of continental crust may be small compared to mantle outgassing (*e.g.*, Sarda et
122 al., 1985). Using constraints from ancient atmospheric Ar composition in a model of Earth's
123 thermal evolution and Ar outgassing history, Guo and Korenaga (2020) suggested that atmospheric
124 Ar isotope evolution was strongly sensitive to continental crust growth primarily through mantle
125 melting to generate continental crust, and to a lesser extent through crustal recycling and reworking.

Guo and Korenaga argued for intense early crustal growth that reached >80% of present-day continental crust volume during the early Archean.

All of the existing Ar isotopic models invoking a catastrophic early outgassing stage fail to account for Ne isotope systematics, which provide important constraints on atmospheric volatile origins. ^{20}Ne and ^{22}Ne are primordial isotopes of Ne. As the production of ^{20}Ne or ^{22}Ne is insignificant in the mantle, the mantle $^{20}Ne/^{22}Ne$ ratio is not measurably affected by any radioactive processes. The present-day mantle $^{20}Ne/^{22}Ne$ is high and solar-like (>12.5; Williams and Mukhopadhyay, 2019) compared to the atmosphere (9.8; Eberhardt et al., 1965). Catastrophic early outgassing would have released large amounts of solar-like Ne with high $^{20}Ne/^{22}Ne$ to the atmosphere, and subsequent continuous mantle outgassing would only add Ne with high $^{20}Ne/^{22}Ne$ to the atmosphere. Mass fractionation due to early hydrodynamic atmospheric loss (Lammer et al., 2020; Pepin, 2006), cannot explain the low $^{20}Ne/^{22}Ne$ in the present-day atmosphere: while kinetic atmosphere loss can be driven to match the atmospheric $^{20}Ne/^{22}Ne$, it would yield unsatisfactorily low $^{36}Ar/^{22}Ne$ compared to modern atmosphere (Marty, 2012; Marty, 2022). Rather, the atmospheric primordial Ne and Ar isotope signature is consistent with a mix between delivered primordial volatiles (similar to carbonaceous chondrites) and a small contribution of outgassed mantle volatiles with solar-like compositions (Marty, 2022). Therefore, a new model of noble gas isotopic evolution that takes volatile delivery to the early atmosphere by impact degassing (*e.g.*, Zahnle et al., 1988) into account is needed.

The rich, multidimensional system of information available in mantle and atmospheric noble gas isotopes has yet to be harnessed in a self-consistent model. In order to investigate

147 atmospheric volatile origins, budgets of heat-producing elements in the solid Earth, and crust-
148 mantle-atmospheric differentiation, we present a numerical model of coupled He, Ne and Ar
149 isotopic evolution in the mantle, crust and atmosphere. We explore a wide variety of scenarios and
150 parameters regarding mantle degassing, continental crust growth and initial noble gases in Earth's
151 atmosphere. Our forward model of isotopic evolution identifies combinations of input parameters
152 that successfully reproduce constraints on present-day mantle He and Ar, atmospheric Ne and Ar,
153 and ancient (Archean and Devonian) atmospheric Ar isotopes. For reasonable combinations of
154 geochemical and geophysical parameter values, a simple model of primordial atmospheric delivery,
155 continuous continental crust growth, and mantle outgassing provides model outputs in agreement
156 with all observational constraints. Successful model realizations are found for a wide range of
157 input parameters given a bulk silicate Earth K/U estimate of 13,000; fewer successful parameter
158 combinations are found for higher and lower estimates of this ratio. The coupled He-Ne-Ar isotope
159 systematics provide constraints on initial primordial noble gas abundances in the mantle. We show
160 that atmospheric Ar isotope evolution is primarily controlled by the history of mantle outgassing
161 and is only weakly sensitive to net continental crust growth. Lastly, the results indicate that direct
162 delivery of volatiles by impact degassing is critically important to atmospheric origins, and that
163 contributions from delivery and outgassing can vary widely among volatile species and indeed
164 among isotopes of a given volatile element (*e.g.,* ^{36}Ar and ^{40}Ar).
165
166 **2. Methods**
167 To investigate the long-term co-evolution of the mantle, continental crust and the atmosphere

associated with mantle processing, we use a three box forward model (Figure 1) of noble gas isotopic evolution over the past 4.488 billion years, starting at 80 Myrs after Earth's formation (consistent with the model start time in Parai, 2022). Figure 2 compares our model setup to prior models of mantle outgassing and the evolution of the atmosphere over time. In each time step, we track the outgassing of mantle ^{3}He, ^{4}He, ^{20}Ne, ^{22}Ne, ^{40}Ar and ^{36}Ar to the atmosphere, the net growth of continental crust, the sequestration of incompatible radioactive parent isotopes ^{235}U, ^{238}U, ^{232}Th and ^{40}K from the mantle in the continental crust, and the production of radiogenic nuclides in silicate reservoirs. Our goal is to explore a wide parameter space (Table S1) and find parameter combinations that satisfy constraints on the present-day MORB source He and Ar isotopic ratios and abundances, the present-day atmospheric Ne abundances and ^{20}Ne/^{22}Ne ratios, the present-day atmospheric Ar abundances, and atmospheric ^{40}Ar/^{36}Ar ratios of the present-day and the past (Cadogan, 1977; Pujol et al., 2013; Stuart et al., 2016). Exploring the bulk silicate Earth (BSE) K/U ratio, which affects estimates of the production of radiogenic heat and radiogenic noble gas nuclides ^{4}He and ^{40}Ar in Earth's major geochemical reservoirs, is also key to refining the understanding of the details of mantle-crust-atmosphere evolution. The names, functions, and ranges of these parameters are shown in Table S1. Below we discuss the details of the model setup.

2.1 Box 1: the MORB source mantle

We consider the MORB source mantle as the primary source of outgassed atmospheric noble gases to reduce model complexity (Section 3). The first model parameter is the mass of the MORB source mantle reservoir (M_{res}); we explore the range from 50% to 90% of the total mantle mass.

189 The second parameter is the total number of mantle reservoir masses processed over the past 4.488
190 billion years (N_{res}, ranging from 2 to 15; see SM and Parai and Mukhopadhyay (2018) for further
191 detail).

192 We parameterize the extent and rate of the long-term processing of the MORB mantle based
193 on M_{res} and N_{res}. Mantle outgassing at mid-ocean ridges, depletion of the MORB mantle due to
194 growth of continental crust, and radioactive decay are all processes that continuously alter the
195 MORB source mantle's chemical composition. Equations that track the concentrations of
196 radioactive ^{235}U, ^{238}U, ^{232}Th and ^{40}K, radiogenic ^{4}He and ^{40}Ar, and primordial ^{3}He, ^{20}Ne, ^{22}Ne and
197 ^{36}Ar in the MORB source mantle at a given time are given in the Supplementary Material (SM).

198 We determine the initial budgets of mantle primordial noble gas isotopes by allowing mantle
199 ^{3}He initial abundances to vary from 1×10^{9} to 1×10^{12} atoms/gram, a large range that encompasses
200 estimates from prior studies (Harper and Jacobsen, 1996; Parai and Mukhopadhyay, 2018; Parai,
201 2022). Corresponding initial mantle abundances of ^{22}Ne are determined using a depleted mantle
202 ^{3}He/^{22}Ne ratio of 10 (Tucker and Mukhopadhyay, 2014). As the initial mantle ^{20}Ne/^{22}Ne is debated
203 (Trieloff et al., 2000; Holland and Ballentine, 2006; Jaupart et al., 2017; Williams and
204 Mukhopadhyay, 2019), the MORB mantle ^{20}Ne/^{22}Ne is treated as a stable isotope ratio fixed at the
205 modern depleted mantle value of 12.6 (Parai and Mukhopadhyay, 2021). The potential range of
206 initial mantle ^{3}He/^{36}Ar ratios of 1.12 to 1.43 is computed using the depleted mantle ^{36}Ar/^{22}Ne
207 values from 7 to 9 (Marty, 2012). Table S2 gives a summary of noble gas initial abundances and
208 isotope ratios. We use present-day BSE Th abundance of 85.3 ppb and BSE U abundance of 20.3
209 ppb from McCulloch and Bennett (1994). We test two BSE K/U ratios of 13,000 and 19,000, both

anchored to the BSE U abundance=20.3 ppb. The initial mantle ^{40}K, ^{238}U, ^{235}U, and ^{232}Th concentrations are each computed using their respective present-day isotopic abundances and decay constants (Table S3).

We assume that noble gases are perfectly incompatible during partial melting and are degassed completely from the melt. For lithophile elements such as U, Th, and K, the net extraction from the mantle is directly related to the net continental crust growth. The depletion of U, Th and K in the mantle is therefore modeled to track the estimated volume of continental crust in 5 different models (Section 2.2), independent of the mantle processing rate. We note that Guo and Korenaga (2020) erroneously assumed that Parai and Mukhopadhyay (2018) used net continental crust growth rates to calculate mantle degassing rates. That is an inaccurate description of the model of Parai and Mukhopadhyay (2018); that work and the present study both explicitly separate mantle degassing rate history (explored as a function of N_{res} and M_{res}) and prescribed models of net continental crust growth that govern extraction of U, Th and K from the mantle.

2.2 Box 2: the continental crust

We model five plausible scenarios of net growth of continental crust over time (*CC* models, Figure 3). The net growth in the volume of continental crust accounts for both the production of new continental crust, and the destruction of existing continental crust through weathering, erosion, and the subduction of sediments. The first continental crust growth scenario (*CC1*) is based on the model of Fyfe (1978) with rapid crustal growth in late Hadean and Archean in excess of the present-day continental crust volume, followed by net decline of crustal volume to the present.

The second scenario (*CC2*) models rapid growth within the first one billion years of Earth history (Armstrong and Harmon, 1981). The third scenario (*CC3*) is similar to *CC2* except that net continental crust growth begins about 200 Myr after the start of the Solar System, accounting for the latest estimates for the timing of the Moon-forming giant impact (Borg et al., 2011). The fourth scenario (*CC4*) models a relatively even, protracted crustal growth from the start of Earth's history (Belousova et al., 2010; Dhuime et al., 2012; Pujol et al., 2013; Walzer and Hendel, 2017). The fifth scenario (*CC5*) models even, protracted growth that starts later in Earth's history: most of the continental crust is generated after the first 1.5 billion years in this model (Condie, 1998; Poupinet and Shapiro, 2008; Rino et al., 2004).

To determine the net extraction of each incompatible lithophile elements U, Th and K from the MORB mantle to the continental crust, we calculate extraction constants that satisfy mass balance in the bulk silicate Earth for each given combination of M_{res} and *CC* model. Taking into consideration extraction of U, Th, and K from the MORB mantle, the in-situ decay of radiogenic parent isotopes accumulating in the continental crust, and crustal degassing, we determine the crustal concentrations of ^{235}U, ^{238}U, ^{232}Th, ^{40}K and ^{40}Ar, with a parameter f that describes the fraction of crustal radiogenic ^{40}Ar degassed to the atmosphere in a given time step (SM).

2.3 Box 3: the atmosphere

The total amounts of ^{20}Ne, ^{22}Ne, ^{36}Ar and ^{40}Ar in the atmosphere at a given time are based on budgets in the previous time step, mantle degassing, and continental crust degassing (Table S4). Accumulation of ^{3}He and ^{4}He in the atmosphere is not tracked, as He escapes to space over time.

252 Catastrophic outgassing from the mantle during accretion and impact degassing of chondritic
253 materials delivered as part of the late veneer would both contribute Ar with low $^{40}Ar/^{36}Ar$ to the
254 early atmosphere, but only chondritic delivery can explain both atmospheric Ne and Ar isotopes
255 (Figure 2). Direct delivery of volatiles to the atmosphere by impact degassing (Zahnle et al., 2010,
256 1988) during accretion is an important process (Marty, 2012) that has not previously been
257 accounted for in models of atmospheric noble gas isotopic evolution. In our model, the total
258 amount of atmospheric Ar from delivery is calculated by assuming no delivered Ar to start, and
259 then computing the amount of delivered Ar needed to give the present-day $^{40}Ar/^{36}Ar$ ratio of 298.6
260 at the end of each model realization. The amount of atmospheric Ne from delivery is calculated
261 using the chondritic $^{22}Ne/^{36}Ar$ ratio (Marty, 2012). Calculations of the amounts of chondritic Ne
262 and Ar delivered to the Earth's atmosphere are described in Table S4. The coupled atmospheric
263 Ar-Ne systematics with delivery and mantle outgassing are constrained by the modern atmospheric
264 $^{20}Ne/^{22}Ne$ ratio, Archean $^{40}Ar/^{36}Ar$ ratio from Pilbara cherts (Pujol et al., 2013), and Devonian
265 atmospheric $^{40}Ar/^{36}Ar$ from Rhynie cherts (Cadogan, 1977; Stuart et al., 2016) to assess model
266 success.

267 Previous studies have demonstrated that atmospheric Ar is injected into the deep mantle via
268 subducted materials (Holland and Ballentine, 2006; Jackson et al., 2013; Parai et al., 2019, 2012;
269 Smye et al., 2017). However, the total amount of regassed Ar in the mantle is uncertain. In our
270 model, if the final amount of atmospheric Ar (outgassed and delivered) exceeds the observed
271 present-day Ar budget, then the excess atmospheric Ar is deducted from the atmosphere box and
272 added to the MORB source mantle box as regassed atmospheric Ar (Table S4). The regassed Ar is

assumed to have the modern atmospheric $^{40}Ar/^{36}Ar$ ratio and has an impact on the calculated present-day $^{40}Ar/^{36}Ar$ ratio of the MORB source mantle, which is compared to the estimate of the present-day MORB source mantle $^{40}Ar/^{36}Ar$ ratio (Moreira et al., 1998; Parai et al., 2012; Parai and Mukhopadhyay, 2021).

2.4 Input parameters and criteria for model success

We explore three parameters (Table S1) using a simple Monte Carlo sampling method to seek the bounds on a successful parameter space: the initial mantle ^{3}He abundance, the mantle $^{3}He/^{36}Ar$ ratio, and the crustal degassing parameter *f*. Four other parameters are explored using discrete test values (M_{res}, N_{res}, *CC* model and the BSE K/U ratio) to examine the effect of varying these parameters (Table 1) on the successful parameter space. For each tested BSE K/U scenario (including a common estimate of 13,000 and higher estimate 19,000; Jochum et al., 1983; Arevalo et al., 2009; Gale et al., 2013), the model draws random values from a range with a uniform distribution for the three Monte Carlo parameters and performs parallel computations of isotopic evolution for discrete combinations of M_{res}, N_{res}, *CC* model. Table S1 gives the ranges tested for each parameter; model runs were repeated with progressively narrowed input ranges to get a well-defined solution space where possible.

Seven noble gas observational constraints were used to assess model success (Table S5). To identify the combinations of input parameters generating the most satisfactory outputs, a weighted scoring system was developed based on residuals between the model outputs and the observational constraints (Table S4). The total score ($Score_{total}$) is a sum of squared residuals normalized to the

uncertainties: the smaller the total score, the better a model realization output meets the observational constraints. Model realizations with $Score_{total}$ smaller than 7 translate to being within one standard deviation (1σ) on average for each of seven tests, and realizations with $Score_{total}$ smaller than 28 are within 2σ on average.

3. Model Results

The model generates time series for He, Ne, Ar, U, Th, and K abundances and He, Ne, and Ar isotopic compositions in the mantle, continental crust and atmosphere. Tables 1 and S1 identify the input parameter ranges that yield successful model realizations as defined above. Below we discuss the modeled isotopic evolution and outcomes compared to model constraints.

The net extraction of incompatible elements U, Th, and K from the MORB source mantle to the continental crust over time is calculated using mass balance (Section 2.2). All but one combination of continental crust growth models and M_{res} can satisfy mass balance for the present-day U and Th concentrations of the continental crust: for the *CC1* model, where the total volume of continental crust once exceeded the present-day volume by about 30%, the smallest M_{res} (50% the total mass of the mantle) would not contain sufficient U and Th. The *CC1* growth model would also require more K than is available even in the largest M_{res} of 90% of the mantle given the largest tested BSE K/U of 19,000 (the combination that maximizes K available to go into the continental crust). This indicates that if large volumes of crust accumulated early in Earth's history (as in *CC1*), that crust cannot have resembled the modern continental crust in its trace element content (*e.g.*, Tucker et al., 2022). Because *CC1* fails to satisfy mass balance for U and K, we do not discuss it

315 further; the rest of the model results and discussion only include models *CC2* to *CC5*.

316 Time evolution of the abundances of ^{238}U, ^{232}Th, and ^{40}K in the MORB source mantle (Figure
317 4) reflects radioactive decay and the progressive depletion of incompatible elements directly
318 reflecting extraction to the growing continental crust. Outgassing of the depleted MORB source
319 mantle is reflected in the increase in $^{4}He/^{3}He$ and $^{40}Ar/^{36}Ar$ ratios over time (Figure 5): all noble
320 gas isotopes are released from the MORB source mantle to the atmosphere due to outgassing
321 during partial melting, but loss of ^{4}He and ^{40}Ar to the atmosphere is counterbalanced by ingrowth
322 from the in-situ decay of radioactive U, Th and K isotopes in the MORB source mantle. Higher
323 mantle processing rates (corresponding to higher numbers of reservoir masses processed over
324 Earth history, N_{res}) will lead to significantly more radiogenic noble gas isotopic signatures in the
325 MORB source mantle reservoir at a given timestep, as well as larger total amounts of mantle ^{40}Ar
326 outgassed to the atmosphere. For model realizations where the resulting atmospheric ^{40}Ar budget
327 exceeds what is observed, atmospheric Ar must have been regassed into the mantle to compensate
328 (Figure 5).

329 MORB source mantle $^{4}He/^{3}He$ ratios and $^{40}Ar/^{36}Ar$ ratios at the present-day for successful
330 model realizations ($Score_{total}<28$) are compared with present-day observational constraints (Figure
331 6). Among successful model scenarios, we found both some that require Ar regassing and others
332 with no regassing of Ar (Figure S1). Most of the successful simulations fall in the range of 80,000
333 to 100,000 for the MORB source mantle $^{4}He/^{3}He$ ratio (Graham, 2002), and 24,000 to 40,000 for
334 the $^{40}Ar/^{36}Ar$ ratio (Figure 6; Holland and Ballentine, 2006; Moreira, 1998; Parai and
335 Mukhopadhyay, 2021). In successful model realizations, 98-99% of primordial noble gas budgets

are lost from the mantle by continuous outgassing. The outgassing rates for ^{36}Ar over time are shown in Figure S2.

Atmospheric $^{20}Ne/^{22}Ne$ and $^{40}Ar/^{36}Ar$ ratios are tracked from an initial composition similar to chondrites (Marty, 2022, 2012) to the present-day compositions. For atmospheric Ne isotopes, only the initial and present-day compositions are constrained. For $^{40}Ar/^{36}Ar$, additional constraints are available in the Archean and Devonian. $^{40}Ar/^{36}Ar$ time series in successful model realizations show that although both BSE K/U of 13,000 and 19,000 can generate past atmospheric Ar isotopic compositions that are consistent with measurements from Archean and Devonian samples (Figure 7), a relatively narrow set of input parameters yields success for high BSE K/U.

We note that while the model explores the contribution of Ar from the upper mantle with 50-90% of total mantle mass (M_{res}), it does not track the isotopic evolution of the plume source mantle or its contributions to the atmosphere by degassing. For *CC* models with early crustal growth (*CC2* and *CC3*), successful model realizations are found with M_{res} of 90%, in which case the plume mantle is only 10% of total mantle mass and makes a relatively small outgassing contribution to the atmosphere. For CC models with late crustal growth (*CC4* and *CC5*), successful model realizations are only found with relatively low M_{res} (62.5%; Figure S3); given the model setup, the rest of the mantle is not outgassed. Parai (2022) found that while the plume mantle is less degassed than the MORB source mantle, it is an open system that has experienced significant outgassing. The late crustal growth scenarios likely would no longer satisfy atmospheric Ne and Ar observational constraints if degassing of the rest of the mantle were taken into account.

4. Discussion

The three-reservoir box model identifies combinations of parameters that enable good fits to all observational criteria. By accounting for delivery of chondritic noble gases, mantle outgassing and atmospheric regassing of volatiles, our model setup provides successful isotopic evolution paths and budgets simultaneously for He, Ne, and Ar in the mantle and atmosphere. Below we discuss the impact of considering atmospheric Ne isotopes, and the implications of our model on Earth's initial volatile budgets, continental crust growth, the bulk silicate Earth K/U ratio, and the coupled evolution of the terrestrial atmosphere, crust, and mantle over time.

4.1 The initial terrestrial noble gas budgets

The initial budgets of primordial He and Ar in the mantle were established during accretion. Primordial isotope ratios in the mantle are consistent with a mixture of He- and Ne-rich solar nebular gas (likely ingassed into a magma ocean) with a planetary component relatively rich in Ar, Kr and Xe, similar to chondrites (Broadley et al., 2022; Parai, 2022; Parai and Mukhopadhyay, 2021; Péron et al., 2021; Williams and Mukhopadhyay, 2019). Catastrophic mantle outgassing due to giant impacts affected primordial noble gas budgets through the end of accretion. Harper and Jacobsen (1996) computed an initial mantle ^{3}He budget assuming closed system evolution from solar He composition to the present-day composition of the less processed mantle component sampled at ocean islands. However, this estimate is a lower limit; any mantle outgassing would require higher initial ^{3}He concentrations to compensate. An upper limit can be determined by combining He and Xe isotope systematics to find an upper bound on N_{res} for the MORB source

mantle ((Parai and Mukhopadhyay, 2018; Parai, 2022).

Our model explores the abundance of mantle ^{3}He at the end of accretion (taken to be 80 Myrs after the start of the Solar System) as an input parameter, which then ties to the initial budgets of ^{22}Ne and ^{36}Ar respectively using the mantle $^{3}He/^{22}Ne$ ratio (Tucker and Mukhopadhyay, 2014) and a relatively narrow range of potential mantle $^{3}He/^{36}Ar$ ratios to account for the possible regassing of atmosphere ^{36}Ar. The initial ^{3}He budget needs to satisfy coupled He-Ne-Ar constraints in multiple reservoirs. When the initial mantle ^{3}He concentration is high, more vigorous mantle outgassing is needed to satisfy the present-day observed upper mantle $^{4}He/^{3}He$. However, a high initial mantle ^{3}He concentration directly translates to a high initial mantle ^{22}Ne concentration. With enhanced mantle outgassing and high mantle noble gas abundances, the MORB source mantle would outgas more Ne with high $^{20}Ne/^{22}Ne$ to the atmosphere, which would yield present-day atmospheric $^{20}Ne/^{22}Ne$ ratios higher than observed. Consideration of atmospheric Ne and Ar isotopes thus enables a stricter constraint on initial mantle ^{3}He.

Successful model realizations ($Score_{total}<28$) with BSE K/U=13,000 are found with initial mantle ^{3}He concentrations from 1.0 to 2.5×10^{11} atoms/gram. Realizations with $Score_{total}<7$ occur in a narrower initial ^{3}He range of 1.2 to 2.1×10^{11} atoms/gram (Table 1). For realizations with BSE K/U=19,000, successful initial mantle ^{3}He has a tighter range of 2.2 to 2.7×10^{11} atoms/gram (Table S1). These ranges are consistent with MORB source mantle initial ^{3}He concentrations in successful scenarios from the coupled He-Ne-Xe model of Parai (2022). Compared with the prior lower limit of 7.8×10^{10} atoms/gram (Harper and Jacobsen, 1996) and upper bound of 8.0×10^{12} atoms/gram inferred from Xe isotope systematics (Parai and Mukhopadhyay, 2018), the model significantly

399 narrows down the estimate of initial mantle ^{3}He that would be retained in the mantle at the end of
400 the accretion (and corresponding ^{22}Ne and ^{36}Ar) by leveraging combined He-Ne-Ar isotope
401 systematics. This has implications for the pressure of the nebular atmosphere in equilibrium with
402 the terrestrial magma ocean, and for the amount of gas retained through the giant impact stage of
403 the accretion.
404
405 *4.2 Atmospheric Ar isotopes are controlled by mantle outgassing and are only weakly sensitive to*
406 *growth of the continental crust*
407 The timing and rate of net continental crust growth influence the abundance and isotopic
408 composition of Ar outgassed from the MORB mantle to the atmosphere and crustal ^{40}Ar outgassed
409 to the atmosphere. Prior studies have argued that ancient and present-day records of atmospheric
410 ^{40}Ar/^{36}Ar are proxies for continental crust growth over time (*e.g.*, Pujol et al., 2013; Stuart et al.,
411 2016; Guo and Korenaga, 2020).
412 Figure 8a shows atmospheric ^{40}Ar/^{36}Ar ratio time series for the model realization with the
413 lowest $\text{Score}_{\text{total}}$, along with a set of curves generated by varying the *CC* model while holding all
414 other model parameters constant. Variation of the *CC* model generates only minor differences in
415 atmospheric ^{40}Ar/^{36}Ar ratio time evolution, with variations manifesting most strongly before ~2.5
416 Ga. Compared to models with more gradual net continental crust growth that started later into
417 Earth history (*CC4* and *CC5*), models with early, rapid net continental crust growth during Hadean
418 and Archean (*CC2* and *CC3*) show slightly higher atmospheric ^{40}Ar/^{36}Ar ratios early in Earth's
419 history due to crustal outgassing (~2% more at ~1 Gyr after the start). However, differences

between atmospheric $^{40}Ar/^{36}Ar$ time series for different *CC* models (with all other parameters kept the same) are small compared to the uncertainties reported for the paleo-atmospheric $^{40}Ar/^{36}Ar$ ratio (on the order of ~10%; Pujol et al., 2013). The existing atmospheric Ar isotopic record thus has little power to distinguish among crustal growth models.

We find instead that the mantle processing rate history exerts primary control on the evolution of atmospheric $^{40}Ar/^{36}Ar$, as this history dictates the rate of outgassing of highly radiogenic mantle Ar to the atmosphere over time (Figure 8b). Our model setup assumes an exponentially decreasing mantle processing rate. A linearly decreasing processing rate and a constant rate are shown for comparison, which yield significantly larger (~7% and ~24% respectively) variations at 1 Gyr after the start than the ~2% differences generated by continental crust growth models (Figure 9). The geochemical-geodynamical model of Tucker et al. (2022) gives atmospheric $^{40}Ar/^{36}Ar$ over time with either constant convective vigor or enhanced early convective vigor, corresponding to processing rates that are near-constant or linearly decreasing. Our results demonstrate that Tucker et al. (2022) yielded significantly lower Archean atmospheric $^{40}Ar/^{36}Ar$ than the observed because their mantle processing rates are too low in the past. Instead, the mantle processing rate must have decreased near-exponentially over time.

Guo and Korenaga (2020) presented a model in which the total mantle processing rate is split into three components: mantle processing to generate oceanic crust, to generate hotspots, and to generate continental crust. The authors presented results in which atmospheric ^{40}Ar contributions from mantle melting to generate the continental crust far exceed any other contributing flux, including ^{40}Ar from mantle processing at mid-ocean ridges, both in a cumulative sense and at any

441 instantaneous point in Earth's history after initiation of crustal growth. It is difficult to envision
442 how mantle processing to generate continental crust could contribute twice the instantaneous flux
443 of ^{40}Ar to the atmosphere as that from melting at mid-ocean ridges even in the present-day (Figure
444 4 in Guo and Korenaga, 2020). Nonetheless, the dominant ^{40}Ar contribution suggested by Guo and
445 Korenaga (2020) is still derived from mantle outgassing, which is consistent with our result.

446 We note that Guo and Korenaga (2020) also argued that crustal recycling and reworking
447 contributed considerable proportions (~25%) of atmospheric ^{40}Ar. In our model, all crustal ^{40}Ar
448 contributions are captured via the crustal degassing coefficient, *f*. The proportion of atmospheric
449 ^{40}Ar with a crustal outgassing origin was computed (Figure S4) for all model simulations with
450 $Score_{total}$<7. Crustal outgassing accounts for ~3 to 6% of atmospheric ^{40}Ar with a late onset of net
451 crustal volume increase (*CC4* and *CC5*), while *CC* models with net crustal growth starting early
452 (*CC2* and *CC3*) can provide up to 13% of the present-day atmospheric ^{40}Ar, similar to the estimate
453 from Sarda et al. (1985). The discrepancy potentially stems from the lack of consideration in Ne
454 isotope systematics in Guo and Korenaga (2020). To explain the atmosphere Ne abundance and
455 ^{20}Ne/^{22}Ne ratio, outgassing of mantle-derived Ne to the atmosphere is required, which
456 simultaneously transports mantle ^{40}Ar to the atmosphere. Without taking atmospheric Ne isotopes
457 and abundances into account, crustal contributions to atmospheric ^{40}Ar can be overestimated.
458 Invoking hypothetical catastrophic early mantle outgassing also drastically decreases the average
459 ^{40}Ar/^{36}Ar of the integrated Ar contribution from mantle outgassing, leading to the overestimation
460 of ^{40}Ar contribution from crustal processes.

461 Our model uses He-Ne-Ar systematics to provide new constraints on mantle outgassing rates,

462 which in turn limits the potential range of crustal degassing rates. For $Score_{total}<7$ model
463 realizations with BSE K/U of 13,000, the crustal degassing coefficient must be smaller than
464 2.05×10^{-9} yr^{-1} and larger than 1.98×10^{-11} yr^{-1}. For $Score_{total}<28$ model realizations with BSE
465 K/U=19,000, the crustal degassing rate is constrained to a much narrower range of $1.85\text{-}1.89\times10^{-10}$ yr^{-1}. In both tested BSE K/U scenarios, the extent of crustal degassing of successful model
467 realizations is broadly consistent with the crustal degassing coefficient estimate of 3.7×10^{-10} yr^{-1}
468 (Hamano and Ozima, 1975). The apparent narrow range of crustal degassing coefficients for
469 successful BSE K/U=19,000 simulations is likely caused by the limited combinations of *CC*
470 models, MORB source mantle reservoir mass, and mantle outgassing rate (Table S1, Figure S3)
471 that simultaneously accommodate for high K abundances while satisfying tight constrains from
472 He and Ne isotope systematics.

473 Overall, instead of crustal growth and degassing, mantle outgassing is the dominant process
474 that transports ^{40}Ar to the atmosphere. Therefore, we caution against using atmospheric $^{40}Ar/^{36}Ar$
475 to reconstruct continental crust growth over time (Figure 8a). Instead, archives of ancient
476 atmospheric $^{40}Ar/^{36}Ar$ have a greater potential to shed light on past mantle processing rates.

477

478 *4.3 The BSE K/U ratio*

479 The BSE K/U ratio has crucial implications for accretionary processes that led to the depletion
480 of terrestrial moderately volatile elements (MVE) compared to chondritic precursors (Wang et al.,
481 2021), terrestrial radiogenic heat production, and compositional evolution of the mantle and
482 atmosphere through outgassing. Although K and U behave similarly during silicate partial melting,

it is challenging to estimate the terrestrial BSE K/U ratio. One complexity comes from dehydration reactions at subduction zones that fractionate the more fluid-mobile element K from U (Becker et al., 2000, Hanyu et al., 2011; Lassiter et al., 2003). Recycled oceanic crust and lithosphere that are not yet well-mixed into the ambient mantle could lower estimates of BSE K/U computed from weighted averages inferred from globally sampled MORBs, OIBs, and continental crust. Neither the mass of isolated patches of recycled materials nor the extent of K/U fractionation in subduction zone settings is well-understood, which generates uncertainties in mass balance among major silicate reservoirs. Based on the existing global K/U datasets, recent studies have accounted for effects of K/U fractionation to infer magma source K/U compositions (Farcy et al., 2020) or have decreased uncertainty from terrestrial K/U fractionation by filtering global oceanic and continental crust datasets, selecting only those with similar relative abundances of strongly incompatible lithophile refractory elements compared to CI chondrites (Dauphas et al., 2022).

Most recent BSE K/U estimates fall between ~10,000 and 14,000 (Arevalo et al., 2009; Dauphas et al., 2022; Farcy et al., 2020; Gale et al., 2013; Jochum et al., 1983; O'Neill et al., 2020; Palme and O'Neill, 2013). However, we explored the extreme case where K/U is not fractionated by partial melting and the BSE K/U is the same as the MORB source mantle estimate of 19,000 (Arevalo et al., 2009). Model success is affected by the choice of BSE K/U ratio, and strongly depends on the corresponding combined choices of other parameters including N_{res}, M_{res}, and continental crust growth model.

For both high (=19,000) and low (=13,000) BSE K/U ratios, we identify model realizations that meet all observational constraints (Table S1, Figure S3). Given the same total number of

simulations, a high BSE K/U=19,000 generates a very limited number of successful ($Score_{total}$<28) model realizations with a very restricted range of input parameters (Table S1). For BSE K/U=13,000, fine tuning of the other model parameters is not necessary for generating model success, and the minimum total scores are lower, indicating better overall fits. We also explored an even lower estimate of BSE K/U=9,000, which produces some successful model realizations (Table S1; Figure S5). Decreased ^{40}Ar production in silicate reservoirs leads to smaller amounts of chondritic Ar and Ne delivery allowed to explain atmospheric Ar composition, which means limited mantle Ne with high $^{20}Ne/^{22}Ne$ can be outgassed to the atmosphere. As a result, only low mantle outgassing rates can be tolerated, which yield lower atmospheric ^{40}Ar abundances than observed. Overall, our model finds the greatest number of successful realizations using a moderate BSE K/U=13,000.

4.4 The origin and evolution of atmospheric Ar and Ne

Three sources with distinct Ne and Ar isotopic compositions contribute to the present-day atmosphere: (1) impact degassing of chondritic materials with low $^{20}Ne/^{22}Ne$, low $^{40}Ar/^{36}Ar$, and high $^{36}Ar/^{22}Ne$ ratios delivered; (2) outgassing to the atmosphere from the MORB source mantle with a solar-like high $^{20}Ne/^{22}Ne$ ratio and progressively increasing $^{40}Ar/^{36}Ar$ ratio over time; and (3) degassing of ^{40}Ar produced in-situ by the decay of ^{40}K in the continental crust. We note that our model approach of combining He, Ne and Ar systematics enables distinction between the different processes contributing to the atmospheric composition over time (Figure 2).

Model realizations with $Score_{total}$<7 indicate that the amount of ^{36}Ar contributed by the delivery

of chondritic materials accounts for 87% to 91% of present-day atmospheric ^{36}Ar after accounting for regassing to the mantle. Thus, our model supports primordial isotope arguments that chondritic Ar delivered to Earth's atmosphere dominates the present-day atmospheric ^{36}Ar budget (Marty, 2012; Broadley et al., 2022), instead of an early stage of catastrophic mantle outgassing and provides a range on the relative proportions of outgassed and delivered ^{36}Ar. In contrast, more than 87% of atmospheric ^{40}Ar is outgassed from the mantle. It is thus important to note that for different atmospheric elemental and isotopic species (in this case, ^{36}Ar and ^{40}Ar), there are distinct breakdowns in the contribution from degassing or chondritic delivery. Given the model estimate of ~4.8 to 5.0×10^{15} moles of ^{36}Ar contributed to the atmosphere through chondritic delivery, ~1.5 to 1.6×10^{22} moles of ^{14}N would be delivered to the atmosphere at the same time assuming a chondritic ^{36}Ar/^{14}N of about 3.2×10^{-7} (Bogard et al., 1971; Marty, 2012; Mazor et al., 1970). Chondritic delivery could thus contribute two orders of magnitude more nitrogen than is presently in the atmosphere. The excess delivered nitrogen may have been dissolved into a more reducing early mantle (Kadik et al., 2011), sequestered in the core at high pressures (Kadik et al., 2011; Roskosz et al., 2013), or progressively sent back to the mantle via subduction (*e.g.*, Bekaert et al., 2021; Stüeken et al., 2016). No nitrogen contribution from mantle outgassing to the atmosphere is required to account for the most abundant species in the present-day atmosphere. Therefore, the common notion that the terrestrial atmosphere was outgassed from the mantle may be inaccurate.

The time evolution of atmospheric ^{20}Ne/^{22}Ne and ^{40}Ar/^{36}Ar ratios for successful model realizations ($Score_{total}$<7) is shown in Figure 10. The model atmospheric ^{20}Ne/^{22}Ne ratio starts at 8.9 (similar to Ne in CI chondrites, Williams and Mukhopadhyay, 2019; Table S3) and increases

546 to the present-day value of 9.8±0.16, with ~90% of the increase occurring in the first Gyr.
547 Atmospheric $^{40}Ar/^{36}Ar$ ratio starts at 0.1 (estimated for CI chondrites based on Ott, 2002) and rises
548 to the present-day value of 298.6, but only 33% of the increase took place in the first Gyr. This is
549 because the increase in atmospheric $^{20}Ne/^{22}Ne$ ratio is only sensitive to the rate of mantle
550 outgassing, which decays exponentially over time (Table S4), whereas a combination of processes
551 including mantle outgassing and the decay of ^{40}K in the MORB source mantle and continental
552 crust all contribute to increases in the atmospheric $^{40}Ar/^{36}Ar$ ratio. Our model indicates that, given
553 the current precision attainable with noble gas mass spectrometers, it would be more difficult to
554 resolve past atmospheric $^{20}Ne/^{22}Ne$ ratios from the present compared to $^{40}Ar/^{36}Ar$ in post-Archean
555 rocks. Our model predicts an Archean atmospheric $^{20}Ne/^{22}Ne$ ratio of around 9.7. This value is >1%
556 lower than the modern ratio (9.8) and could be detected given current analytical precision in
557 $^{20}Ne/^{22}Ne$ (*e.g.*, Parai and Mukhopadhyay, 2021). Future high-precision measurements of ancient
558 Ne and Ar will thus provide further model constraints to refine our understanding of the
559 geophysical parameters that have exerted strong control on volatile transport throughout Earth's
560 history.
561
562 **5. Conclusion**
563 We developed a forward model of noble gas abundances and isotopic evolution in the MORB
564 source mantle, continental crust, and the atmosphere. We investigated initial terrestrial budgets of
565 noble gases and long-lived radioactive lithophile elements, as well as histories of mantle
566 processing and continental crust growth. We explored a wide parameter space and evaluated model

567 realizations by implementing a scoring system based on present-day and ancient (Archean and
568 Devonian) observational constraints on noble gas isotopic compositions in the mantle and
569 atmosphere. The three-reservoir model can simultaneously account for mantle He, Ne, Ar as well
570 as atmospheric Ne and Ar abundances and isotopic compositions and provide insight into initial
571 budgets, atmospheric chondritic noble gas delivery, and long-term mantle outgassing. We are able
572 to narrowly estimate Earth's mantle initial budget of ^{3}He to 1.0-2.5×10^{11} atoms/gram, providing a
573 basis for future evaluation of the retention of nebular gas throughout the accretion process. Our
574 model outcomes demonstrate that the atmospheric ^{40}Ar/^{36}Ar ratio is largely insensitive to histories
575 of continental growth and instead records primarily the mantle processing rate history. The pairing
576 of radiogenic ^{4}He and ^{40}Ar provides a novel way to investigate the BSE K/U ratio. An estimate of
577 BSE K/U of 13,000 satisfies model observational constraints for a wide range of other input
578 parameters. Model results also suggest that the ^{20}Ne/^{22}Ne ratio of atmospheric neon evolved with
579 time with a predicted Archean atmospheric ^{20}Ne/^{22}Ne ratio of around 9.7. We find that chondritic
580 delivery is the major contributor of atmospheric primordial ^{36}Ar instead of mantle outgassing
581 throughout Earth history. Ample nitrogen would be delivered along with ^{36}Ar by impact degassing
582 to account for the present-day atmospheric nitrogen inventory. Future efforts to combine the full
583 suite of noble gases, including Kr and Xe, would further constrain mantle outgassing and the
584 atmospheric evolution over time.
585
586 **Acknowledgments**
587 We thank Rajdeep Dasgupta for efficient editorial handling and Philippe Sarda for constructive

588 comments that improved the manuscript. We gratefully acknowledge the McDonnell Center for
589 the Space Sciences for support to XJZ. This work constituted XJZ's senior honors thesis and was
590 supported by Department of Energy National Nuclear Security Administration grant DENA003911
591 to RP.

592

593 Main text: 7356 words

594

Main Text Figure captions:

Figure 1. **Schematic diagram of the three-box model**. The three geochemical reservoirs of concern are the MORB source mantle, continental crust and the atmosphere. Incompatible lithophile elements U, Th and K are transported to the growing continental crust (controlled by model parameters *CC* and M_{res}). Through partial melting of the MORB source mantle, noble gas isotopes are lost to the atmosphere (controlled by M_{res} and N_{res}). Long-term decay of U, Th and K takes place in the MORB source mantle and the continental crust, leading to in-situ ingrowth of radiogenic daughter isotopes ^{4}He and ^{40}Ar. Part of the ^{40}Ar produced in the continental crust reservoir is lost to the atmosphere, controlled by the crustal degassing parameter *f*. Oceanic crust is omitted in this model due to its negligible mass and impact on Ar production. Reservoir sizes shown are not to scale.

Figure 2. Conceptual model setup for mantle outgassing and atmosphere evolution over time. Catastrophic outgassing of the mantle occurred during the giant impact phase of accretion. Prior models intended to explain the present-day atmospheric ^{40}Ar/^{36}Ar through the retention of Ar outgassed from the mantle during the catastrophic outgassing stage. However, retention of such gases, which have solar-like high ^{20}Ne/^{22}Ne, would fail to yield the low present-day atmospheric ^{20}Ne/^{22}Ne without invoking mass fractionation that would generate an overly low ^{36}Ar/^{22}Ne ratio (Marty, 2012, 2022). Therefore, the model assumes that such gases released during accretion were lost to space during the giant impact stage. Instead, the model accounts for the delivery of

chondritic volatiles to the atmosphere by impact degassing of the late veneer (Zahnle et al., 1988, 2010) and mantle outgassing over time after the last giant impact. The mantle outgassing rate at ridges decreases exponentially with time. Mantle $^{20}Ne/^{22}Ne$ remains the same while $^{40}Ar/^{36}Ar$ increases over time due to mantle outgassing and the decay of ^{40}K. The model accounts for the atmosphere Ne and Ar compositions, and subsequently provides constraints on chondritic delivery and continuous mantle outgassing through the combined He-Ne-Ar systematics.

Figure 3. **Tested models of net continental crust growth over time.** *CC1* (green), *CC2* (red), and *CC3* (yellow) feature various types of early rapid crustal growth. *CC1* reached ~130% of today's continental crust volume, which is followed by a net decrease of continental crust volume over the past 2 billion years (Fyfe, 1978); *CC2* and *CC3* test different timings of net crustal growth initiation based on Armstrong and Harmon (1981); *CC4* (blue) and *CC5* (purple) simulate two different sigmoidal curves where net continental crust growth both continue into later stages in Earth history (*CC4*: Belusova et al., 2010; Dhuime et al., 2012; Pujol et al., 2013; Walzer and Hendel, 2017; *CC5*: Condie, 1998; Poupinet and Shapiro, 1998; Rino et al., 2004).

Figure 4. **Time evolution of MORB source mantle ^{238}U, ^{232}Th, and ^{40}K abundances.** The MORB source mantle is assumed have a BSE starting composition. Abundances of (a) ^{238}U, (b) ^{232}Th, and (c) ^{40}K in the MORB source mantle decrease with time due to extraction and radioactive decay. Green dashed curves show the isolated effect of radioactive decay. U, Th, and K are also extracted from the model MORB source mantle reservoir to the growing continental crust,

637 depleting the MORB mantle of incompatible elements over time (see Supplementary Material for
638 model mass balance setup). Orange and purple time series are produced with continental crust net
639 growth models *CC3* and *CC5*, respectively, with $M_{res,}$ (mass of the MORB source mantle reservoir)
640 equal to 90% of the total mantle mass.
641
642 **Figure 5. Time evolution of MORB source mantle (a) $^{4}He/^{3}He$ and (b) $^{40}Ar/^{36}Ar$ ratios with**
643 **variation in mantle processing rates.** He isotopes start at the solar composition ($^{3}He/^{4}He$=120
644 R_A, where R_A is today's atmospheric $^{3}He/^{4}He$ ratio; Mahaffy, 1998). The mantle $^{40}Ar/^{36}Ar$ ratio
645 initiates at an estimated chondritic value of 0.1 (Ott, 2002). MORB source mantle $^{4}He/^{3}He$ and
646 $^{40}Ar/^{36}Ar$ increase with time because all He and Ar isotopes are lost to the atmosphere upon mantle
647 partial melting but only radiogenic ^{4}He and ^{40}Ar accumulate over time owing to the decay of
648 radioactive ^{235}U, ^{238}U, ^{232}Th, and ^{40}K. For each simulation, regassing of Ar is invoked only if the
649 model present-day atmospheric ^{40}Ar abundance is higher than the model constraint (Table S5). The
650 present-day mantle $^{40}Ar/^{36}Ar$ ratios after the regassing calculation are shown as squares. Time
651 evolution curves are color-coded by N_{res} (the number of reservoir masses processed in the past
652 4.488 Gyr), which characterizes mantle processing rates. As the color changes from purple to
653 orange, N_{res} increases from 3 to 6. For N_{res} = 3 (purple), mantle $^{4}He/^{3}He$ and $^{40}Ar/^{36}Ar$ are too low
654 (demonstrating a failed model realization), and the atmospheric ^{40}Ar abundance is less than
655 observed such that no regassing is invoked. When N_{res} is larger, the present-day MORB source
656 mantle is more processed and outgassed, and the MORB source mantle has a significantly higher
657 $^{4}He/^{3}He$ ratio (a). For the larger N_{res} values shown here (4.05, 5 and 6), outgassed Ar is

658 overabundant and some amount of Ar regassing is needed to match the present-day atmospheric
659 ^{40}Ar abundance constraint. For N_{res} = 4.05 (light blue; success), mantle ^{4}He/^{3}He and mantle
660 ^{40}Ar/^{36}Ar after regassing both match observational constraints at the present-day. For N_{res} = 5 and
661 6 (green and orange), a greater amount of atmospheric regassing leads to mantle ^{40}Ar/^{36}Ar after
662 regassing that are too low compared to the present-day mantle ^{40}Ar/^{36}Ar constraint. Variations in
663 mantle processing rate create a large range of modeled ^{4}He/^{3}He and ^{40}Ar/^{36}Ar evolution curves
664 over time, and exert determining constraints on model successes.
665
666 **Figure 6. Present-day MORB source mantle ^{4}He/^{3}He and ^{40}Ar/^{36}Ar (with regassed Ar) ratios**
667 **from Score$_{total}$<28 simulation outputs.** Each dot represents the present-day MORB source mantle
668 ^{4}He/^{3}He ratio and the present-day MORB source mantle ^{40}Ar/^{36}Ar ratio (including the regassed
669 atmospheric Ar) for one model realization. Dots are color-coded by Score$_{total}$, from the lowest
670 (darkest blue, best performance) up to 28 (lightest blue; see Section 2.4). The rectangle shows
671 observational constraints for both ratios: the present-day MORB source mantle ^{4}He/^{3}He ratio
672 ranging from 80,000 to 100,000 (Graham, 2002) and the present-day MORB source mantle
673 ^{40}Ar/^{36}Ar ratio ranging from ~24,000 (Parai and Mukhopadhyay, 2021) to ~40,000 (Holland and
674 Ballentine, 2006). The dense cluster of dots in the upper left of panel (a) are model realizations
675 that do not invoke any regassing of atmospheric Ar (Figure S1). Mantle outgassing and decay of
676 ^{235}U, ^{238}U, and ^{232}Th influence the present-day MORB source mantle ^{4}He/^{3}He ratio on the x-axis,
677 while outgassing, decay of ^{40}K and regassing of Ar influence the present-day MORB source mantle
678 ^{40}Ar/^{36}Ar ratio on the y-axis. Simulations in panel (a) and (b) are generated using BSE K/U ratio

679 of 13,000 and 19,000 respectively. With a BSE K/U of 19,000, a very restricted set of realizations
680 have $Score_{total}$<28, whereas a BSE K/U of 13,000 yields more successful realizations and better
681 overall fits ($Score_{total}$ as low as 1.16).
682
683 **Figure 7. Time evolution of the atmospheric $^{40}Ar/^{36}Ar$ ratio for successful model simulations.**
684 Blue and red curves are model realizations with $Score_{total}$<28 and $Score_{total}$<7 respectively. The
685 atmosphere is assumed to have a chondrite-like starting $^{40}Ar/^{36}Ar$ ratio, reflecting delivery of
686 atmospheric Ar from accreted material. Outgassing through mantle processing contributes Ar to
687 the atmosphere with the instantaneous mantle $^{40}Ar/^{36}Ar$ ratio, which increases due to degassing
688 and decay of ^{40}K over time. Chondritic delivery also contributes a significant amount of Ar to the
689 atmosphere with a $^{40}Ar/^{36}Ar$ ratio of 0.1. The present-day $^{40}Ar/^{36}Ar$ ratio is anchored at 298.6 (Lee
690 et al., 2006). The orange lines illustrate the bounds on observational constraints for Archean (Pujol
691 et al., 2013) and Devonian (Stuart et al., 2016) atmospheric $^{40}Ar/^{36}Ar$. Simulations in panel (a) and
692 (b) are generated using BSE K/U ratios of 13,000 and 19,000 respectively. Both BSE K/U ratios
693 are able to generate successful simulated atmospheric $^{40}Ar/^{36}Ar$ time evolution series with minimal
694 residuals compared to observations from the Archean and Devonian, but many more successful
695 model realizations are found using the BSE K/U of 13,000.
696
697 **Figure 8. Evolution of the atmospheric $^{40}Ar/^{36}Ar$ ratio with variations in *CC* model, or with**
698 **different mantle processing history.** (a) Atmospheric $^{40}Ar/^{36}Ar$ ratio time evolution curves are
699 generated by using the set of model parameters that generate the smallest $Score_{total}$ and only

varying the choice of *CC* models. Changing the *CC* model generates very similar atmospheric $^{40}Ar/^{36}Ar$ ratio time series. The atmospheric $^{40}Ar/^{36}Ar$ ratio over time is not significantly sensitive to the style of continental crust growth. Other model constraints (*i.e.*, He and Ne) are responsible for the *CC* model selectivity shown in Figure S3. Green lines show the Archean and Devonian atmospheric Ar compositions (Cadogan, 1977; Pujol et al., 2013; Stuart et al., 2016). (b) Atmospheric $^{40}Ar/^{36}Ar$ ratio time evolution curves are generated by using the same set of initial model parameters that generate the lowest $Score_{total}$ and only varying the mantle processing history. The red curve is generated using the exponentially deceasing mantle processing rate pinned to Q_P, the present-day processing rate at mid-ocean ridges (this is the model default; see SM). The dashed curves are similar to mantle processing rates explored in Tucker et al. (2022). The light grey dashed curve reflects a linearly decreasing mantle processing rate pinned at Q_P, with the same integrated mantle processing as the exponentially decreasing scenario (same N_{res}). A linearly decreasing model degrades the fit to Archean constraints, as a less-vigorous early mantle outgassing does not raise the atmospheric $^{40}Ar/^{36}Ar$ ratio fast enough. The dark grey dashed curve, produced by using a constant mantle processing rate Q_P throughout Earth history, does not satisfy any past atmospheric $^{40}Ar/^{36}Ar$ constraints. The rate of continuous mantle outgassing needs to have been significantly higher in the past to explain the change in atmospheric Ar composition over time (Figure S2).

Figure 9. Evolution of atmospheric $^{40}Ar/^{36}Ar$ and $^{20}Ne/^{22}Ne$ ratios in model realizations with $Score_{total}$<7. The atmosphere is assumed to have a chondritic starting composition, reflecting

721 delivery of Ne and Ar from accreted material. Mantle outgassing contributes Ne with higher
722 $^{20}Ne/^{22}Ne$ reflecting solar nebular contributions to the Earth's interior noble gas budget (Williams
723 and Mukhopadhyay, 2019) and contributes Ar with the instantaneous mantle $^{40}Ar/^{36}Ar$, which
724 evolves due to mantle outgassing and decay of ^{40}K over time. Time series are color-coded from
725 light yellow at the start time to dark blue after 4.488 Gyr of evolution starting at 80 Myr after
726 Earth's formation, and magenta squares denote one-billion-year intervals after the start time for
727 each model realization. The model results predict a small but resolvable difference between the
728 Archean atmospheric $^{20}Ne/^{22}Ne$ and the present-day composition. Further measurements of the Ar
729 and Ne isotopic composition of the atmosphere over time will provide a test of the model
730 predictions.
731

References (70 total)

Alexander Jr, E.C. and Ozima, M., 1978. Terrestrial rare gases; Proceedings of the US-Japan Seminar on Rare Gas Abundance and Isotopic Constraints on the Origin and Evolution of the Earth's Atmosphere, Hakone, Kanagawa, Japan, June 28-July 1, 1977. *Advances in Earth and Planetary Sciences*, 3.

Allègre, C., Staudacher, T., Sarda, P., 1987. Rare gas systematics: formation of the atmosphere, evolution and structure of the Earth's mantle. *Earth Planet Sci Lett* 81, 127–150. https://doi.org/10.1016/0012-821X(87)90151-8

Arevalo, R., McDonough, W.F., Luong, M., 2009. The K/U ratio of the silicate Earth: Insights into mantle composition, structure and thermal evolution. *Earth Planet Sci Lett* 278, 361–369. https://doi.org/10.1016/J.EPSL.2008.12.023

Armstrong, R. L. and Harmon, R.S., 1981. Radiogenic isotopes: the case for crustal recycling on a near-steady-state no-continental-growth Earth. *Philosophical Transactions of the Royal Society of London. Series A, Mathematical and Physical Sciences* 301, 443–472. https://doi.org/10.1098/rsta.1981.0122

Avice, G., Marty, B. and Burgess, R., 2017. The origin and degassing history of the Earth's atmosphere revealed by Archean xenon. *Nature communications*, 8(1), p.15455.

Becker, H., Jochum, K.P., Carlson, R.W., 2000. Trace element fractionation during dehydration of eclogites from high-pressure terranes and the implications for element fluxes in subduction zones. *Chem Geol* 163, 65–99. https://doi.org/10.1016/S0009-2541(99)00071-6

Bekaert, D. v., Turner, S.J., Broadley, M.W., Barnes, J.D., Halldorsson, S.A., Labidi, J., Wade, J., Walowski, K.J., Barry, P.H., 2021. Subduction-driven volatile recycling: A global mass balance. *Annu Rev Earth Planet* Sci. https://doi.org/10.1146/annurev-earth-071620-055024

Belousova, E.A., Kostitsyn, Y.A., Griffin, W.L., Begg, G.C., O'Reilly, S.Y., Pearson, N.J., 2010. The growth of the continental crust: Constraints from zircon Hf-isotope data. *Lithos* 119, 457–466. https://doi.org/10.1016/j.lithos.2010.07.024

Bender, M.L., Barnett, B., Dreyfus, G., Jouzel, J., Porcelli, D., 2008. The contemporary degassing rate of 40Ar from the solid Earth. *Proceedings of the National Academy of Sciences* 105, 8232-8237.

Bogard, D.D., Clark, R.S., Keith, J.E., Reynolds, M.A., 1971. Noble gases and radionuclides in Lost City and other recently fallen meteorites. *J Geophys Res* 76, 4076–4083. https://doi.org/10.1029/JB076I017P04076

Borg, L.E., Connelly, J.N., Boyet, M., Carlson, R.W., 2011. Chronological evidence that the Moon is either young or did not have a global magma ocean. *Nature* 2011 477:7362 477, 70–72. https://doi.org/10.1038/nature10328

Broadley, M.W., Bekaert, D.V., Piani, L., Füri, E. and Marty, B., 2022. Origin of life-forming volatile elements in the inner Solar System. *Nature*, *611*(7935), pp.245-255.

Cadogan, P.H., 1977. Palaeoatmospheric argon in Rhynie chert. *Nature* 1977 268:5615 268, 38–41. https://doi.org/10.1038/268038a0

Condie, K.C., 1998. Episodic continental growth and supercontinents: a mantle avalanche

772 connection?. *Earth and Planetary Science Letters*, *163*(1-4), pp.97-108.Crisp, J.A., 1984.
773 Rates of magma emplacement and volcanic output. *Journal of Volcanology and Geothermal*
774 *Research*. https://doi.org/10.1016/0377-0273(84)90039-8
775 Dauphas, N., Nie, N.X., Blanchard, M., Zhang, Z.J., Zeng, H., Hu, J.Y., Meheut, M., Visscher, C.,
776 Canup, R., Hopp, T., 2022. The Extent, Nature, and Origin of K and Rb Depletions and
777 Isotopic Fractionations in Earth, the Moon, and Other Planetary Bodies. *Planet Sci J* 3, 29.
778 https://doi.org/10.3847/PSJ/AC2E09
779 Dhuime, B., Hawkesworth, C.J., Cawood, P.A., Storey, C.D., 2012. A change in the geodynamics
780 of continental growth 3 billion years ago. *Science* (1979) 335, 1334–1336.
781 https://doi.org/10.1126/science.1216066
782 Farcy, B., Arevalo, R., McDonough, W.F., 2020. K/U of the MORB Source and Silicate Earth. J
783 *Geophys Res Solid Earth* 125, e2020JB020245. https://doi.org/10.1029/2020JB020245
784 Farley, K.A., Natland, J.H., Craig, H., 1992. Binary mixing of enriched and undegassed (primitive?)
785 mantle components (He, Sr, Nd, Pb) in Samoan lavas. *Earth Planet Sci Lett* 111, 183–199.
786 https://doi.org/10.1016/0012-821X(92)90178-X
787 Fisher, D.E., 1975. Trapped helium and argon and the formation of the atmosphere by degassing.
788 *Nature*, 256(5513), 113-114.
789 Fyfe, W.S., 1978. The evolution of the earth's crust: Modern plate tectonics to ancient hot spot
790 tectonics? *Chem Geol* 23, 89–114.
791 Gale, A., Dalton, C.A., Langmuir, C.H., Su, Y., Schilling, J.G., 2013. The mean composition of
792 ocean ridge basalts. *Geochemistry, Geophysics, Geosystems* 14, 489–518.
793 https://doi.org/10.1029/2012GC004334
794 Gonnermann, H.M., Mukhopadhyay, S., 2009. Preserving noble gases in a convecting mantle.
795 *Nature* 459, 560-563.
796 Guo, M., Korenaga, J., 2020. Argon constraints on the early growth of felsic continental crust. *Sci*
797 *Adv* 6, 1–11. https://doi.org/10.1126/sciadv.aaz6234
798 Hamano, Y., Ozima, M., 1978. Earth-atmosphere evolution model based on Ar isotopic data, in:
799 *Terrestrial Rare Gases: Proceedings of the U.S.-Japan Seminar on Rare Gas Abundance and*
800 *Isotopic Constraints on the Origin and Evolution of the Earth's Atmosphere*. pp. 155–171.
801 Hanyu, T., Tatsumi, Y., Kimura, J.I., 2011. Constraints on the origin of the HIMU reservoir from
802 He–Ne–Ar isotope systematics. *Earth Planet Sci Lett* 307, 377–386.
803 https://doi.org/10.1016/J.EPSL.2011.05.012
804 Harper, C.L., Jacobsen, S.B., 1996. Noble Gases and Earth's Accretion. *Science* (1979) 273, 1814–
805 1818. https://doi.org/10.1126/SCIENCE.273.5283.1814
806 Heber, V.S., Baur, H., Bochsler, P., McKeegan, K.D., Neugebauer, M., Reisenfeld, D.B., Wieler,
807 R., Wiens, R.C., 2012. Isotopic mass fractionation of solar wind: Evidence from fast and slow
808 solar wind collected by the genesis mission. *Astrophysical Journal*.
809 https://doi.org/10.1088/0004-637X/759/2/121
810 Holland, G., Ballentine, C.J., 2006. Seawater subduction controls the heavy noble gas composition
811 of the mantle. *Nature*. https://doi.org/10.1038/nature04761
812 Jackson, C.R.M., Parman, S.W., Kelley, S.P., Cooper, R.F., 2013. Noble gas transport into the

mantle facilitated by high solubility in amphibole. *Nature Geoscience* 2013 6:7 6, 562–565. https://doi.org/10.1038/ngeo1851

Jaupart, E., Charnoz, S. and Moreira, M., 2017. Primordial atmosphere incorporation in planetary embryos and the origin of Neon in terrestrial planets. *Icarus*, *293*, pp.199-205.

Jochum, K.P., Hofmann, A.W., Ito, E., Seufert, H.M. and White, W.M., 1983. K, U and Th in mid-ocean ridge basalt glasses and heat production, K/U and K/Rb in the mantle. *Nature*, 306(5942), 431-436.

Kadik, A.A., Kurovskaya, N.A., Ignat'ev, Y.A., Kononkova, N.N., Koltashev, V. v., Plotnichenko, V.G., 2011. Influence of oxygen fugacity on the solubility of nitrogen, carbon, and hydrogen in FeO-Na2O-SiO2-Al2O3 melts in equilibrium with metallic iron at 1.5 GPa and 1400°C. *Geochemistry International* 2011 49:5 49, 429–438. https://doi.org/10.1134/S001670291105003X

Lammer, H., Scherf, M., Kurokawa, H., Ueno, Y., Burger, C., Maindl, T., Johnstone, C.P., Leizinger, M., Benedikt, M., Fossati, L., Kislyakova, K.G., Marty, B., Avice, G., Fegley, B., Odert, P., 2020. Loss and Fractionation of Noble Gas Isotopes and Moderately Volatile Elements from Planetary Embryos and Early Venus, Earth and Mars. *Space Sci Rev*. https://doi.org/10.1007/s11214-020-00701-x

Lassiter, J.C., Blichert-Toft, J., Hauri, E.H., Barsczus, H.G., 2003. Isotope and trace element variations in lavas from Raivavae and Rapa, Cook–Austral islands: constraints on the nature of HIMU- and EM-mantle and the origin of mid-plate volcanism in French Polynesia. *Chem Geol* 202, 115–138. https://doi.org/10.1016/J.CHEMGEO.2003.08.002

Lee, J.-Y., Marti, K., Severinghaus, J.P., Kawamura, K., Yoo, H.-S., Lee, J.B., Kim, J.S., 2006. A redetermination of the isotopic abundances of atmospheric Ar. *Geochim Cosmochim Acta* 70, 4507–4512. https://doi.org/10.1016/j.gca.2006.06.1563

Mahaffy, P.R., Donahue, T.M., Atreya, S.K., Owen, T.C., Niemann, H.B., 1998. Galileo probe measurements of D/H and 3He/4He in Jupiter's atmosphere. *Space Sci Rev.* https://doi.org/10.1023/a:1005091806594

Marty, B., 2022. Meteoritic noble gas constraints on the origin of terrestrial volatiles. *Icarus* 381, 115020. https://doi.org/10.1016/J.ICARUS.2022.115020

Marty, B., 2012. The origins and concentrations of water, carbon, nitrogen and noble gases on Earth. *Earth Planet Sci Lett* 313–314, 56–66. https://doi.org/10.1016/j.epsl.2011.10.040

Mazor, E., Heymann, D., Anders, E., 1970. Noble gases in carbonaceous chondrites. *Geochim Cosmochim Acta.* https://doi.org/10.1016/0016-7037(70)90031-1

McLennan, S.M., Taylor, S.R., 1982. Geochemical constraints on the growth of the continental crust. *Journal of Geology.* https://doi.org/10.1086/628690

Moreira, M., Kunz, J., Allègre, C., 1998. Rare gas systematics in popping rock: Isotopic and elemental compositions in the upper mantle. *Science* (1979) 279, 1178–1181. https://doi.org/10.1126/SCIENCE.279.5354.1178/ASSET/9F2E365F-82BB-4677-83AC-018FEC6C9C5F/ASSETS/GRAPHIC/SE0886270005.JPEG

Moreira, M., Raquin, A., 2007. The origin of rare gases on Earth: The noble gas 'subduction barrier'revisited. *Comptes Rendus Geoscience* 339, 937-945.

O'Neill, C., O'Neill, H.S.C., Jellinek, A.M., 2020. On the Distribution and Variation of Radioactive Heat Producing Elements Within Meteorites, the Earth, and Planets. *Space Sci Rev* 216, 1–27. https://doi.org/10.1007/S11214-020-00656-Z/FIGURES/7

Ozima, M., Kudo, K., 1972. Excess Argon in Submarine Basalts and an Earth-Atmosphere Evolution Model. *Nature Physical Science* 1972 239:89 239, 23–24. https://doi.org/10.1038/physci239023a0

Ozima, M., 1975. Ar isotopes and Earth-atmosphere evolution models. *Geochimica et Cosmochimica Acta*, 39(8), 1127-1134.

Palme, H., O'Neill, H., 2013. Cosmochemical Estimates of Mantle Composition, in: T*reatise on Geochemistry: Second Edition*. Elsevier Inc., pp. 1–39. https://doi.org/10.1016/B978-0-08-095975-7.00201-1

Parai, R., 2022. A dry ancient plume mantle from noble gas isotopes. *Proceedings of the National Academy of Sciences* 119, e2201815119. https://doi.org/10.1073/PNAS.2201815119

Parai, R., Mukhopadhyay, S., 2021. Heavy noble gas signatures of the North Atlantic Popping Rock 2ΠD43: Implications for mantle noble gas heterogeneity. *Geochim Cosmochim Acta* 294, 89–105. https://doi.org/10.1016/J.GCA.2020.11.011

Parai, R., Mukhopadhyay, S., 2018. Xenon isotopic constraints on the history of volatile recycling into the mantle. *Nature*. https://doi.org/10.1038/s41586-018-0388-4

Parai, R., Mukhopadhyay, S., Standish, J.J., 2012. Heterogeneous upper mantle Ne, Ar and Xe isotopic compositions and a possible Dupal noble gas signature recorded in basalts from the Southwest Indian Ridge. *Earth Planet Sci Lett* 359–360, 227–239. https://doi.org/10.1016/J.EPSL.2012.10.017

Parai, R., Mukhopadhyay, S., Tucker, J.M., Pető, M.K., 2019. The emerging portrait of an ancient, heterogeneous and continuously evolving mantle plume source. *Lithos* 346–347, 105153. https://doi.org/10.1016/J.LITHOS.2019.105153

Pepin, R.O., 2006. Atmospheres on the terrestrial planets: Clues to origin and evolution. *Earth Planet Sci Lett*. https://doi.org/10.1016/j.epsl.2006.09.014

Péron, S., Mukhopadhyay, S., Kurz, M.D., Graham, D.W., 2021. Deep-mantle krypton reveals Earth's early accretion of carbonaceous matter. 462 *Nature* 600. https://doi.org/10.1038/s41586-021-04092-z

Poupinet, G., Shapiro, N.M., 2008. Worldwide distribution of ages of the continental lithosphere derived from a global seismic tomographic model. *Lithos* 109, 125–130. https://doi.org/10.1016/j.lithos.2008.10.023

Pujol, M., Marty, B., Burgess, R., Turner, G., Philippot, P., 2013. Argon isotopic composition of Archaean atmosphere probes early Earth geodynamics. Nature 498, 87–90. https://doi.org/10.1038/nature12152

Rino, S., Komiya, T., Windley, B.F., Katayama, I., Motoki, A., Hirata, T., 2004. Major episodic increases of continental crustal growth determined from zircon ages of river sands; implications for mantle overturns in the Early Precambrian. Physics of the Earth and Planetary Interiors 146, 369–394. https://doi.org/10.1016/j.pepi.2003.09.024

Roskosz, M., Bouhifd, M.A., Jephcoat, A.P., Marty, B., Mysen, B.O., 2013. Nitrogen solubility in

molten metal and silicate at high pressure and temperature. Geochim Cosmochim Acta 121, 15–28. https://doi.org/10.1016/J.GCA.2013.07.007

Rudnick, R.L., Gao, S., 2003. Composition of the Continental Crust, in: Treatise on Geochemistry. https://doi.org/10.1016/B0-08-043751-6/03016-4

Sarda, P., Staudacher, T. and Allegre, C.J., 1985. 40Ar36Ar in MORB glasses: constraints on atmosphere and mantle evolution. Earth and Planetary Science Letters, 72(4), 357-375.

Smye, A.J., Jackson, C.R.M., Konrad-Schmolke, M., Hesse, M.A., Parman, S.W., Shuster, D.L., Ballentine, C.J., 2017. Noble gases recycled into the mantle through cold subduction zones. Earth Planet Sci Lett 471, 65–73. https://doi.org/10.1016/J.EPSL.2017.04.046

Stuart, F.M., Mark, D.F., Gandanger, P., McConville, P., 2016. Earth-atmosphere evolution based on new determination of Devonian atmosphere Ar isotopic composition. Earth Planet Sci Lett. https://doi.org/10.1016/j.epsl.2016.04.012

Stüeken, E.E., Kipp, M.A., Koehler, M.C., Buick, R., 2016. The evolution of Earth's biogeochemical nitrogen cycle. Earth Sci Rev 160, 220–239. https://doi.org/10.1016/J.EARSCIREV.2016.07.007

Tucker, J.M., Mukhopadhyay, S., 2014. Evidence for multiple magma ocean outgassing and atmospheric loss episodes from mantle noble gases. Earth Planet Sci Lett 393, 254–265. https://doi.org/10.1016/J.EPSL.2014.02.050

Tucker, J.M., van Keken, P.E., Ballentine, C.J., 2022. Earth's missing argon paradox resolved by recycling of oceanic crust. Nature Geoscience 2022 15:1 15, 85–90. https://doi.org/10.1038/s41561-021-00870-6

Walzer, U., Hendel, R., 2017. Continental crust formation: Numerical modelling of chemical evolution and geological implications. Lithos 278–281, 215–228. https://doi.org/https://doi.org/10.1016/j.lithos.2016.12.014

Wang, K., Li, W., Li, S., Tian, Z., Koefoed, P., and Zheng, X. Y., 2021. Geochemistry and cosmochemistry of potassium stable isotopes. Geochemistry, 81(3), 125786.

Williams, C.D., Mukhopadhyay, S., 2019. Capture of nebular gases during Earth's accretion is preserved in deep-mantle neon. https://doi.org/10.1038/s41586-018-0771-1

Zahnle, K., Schaefer, L., Fegley, B., 2010. Earth's Earliest Atmospheres. Cold Spring Harb Perspect Biol 2, a004895. https://doi.org/10.1101/CSHPERSPECT.A004895

Zahnle, K.J., Kasting, J.F., Pollack, J.B., 1988. Evolution of a steam atmosphere during earth's accretion. Icarus 74, 62–97. https://doi.org/10.1016/0019-1035(88)90031-0

927

Figure 1

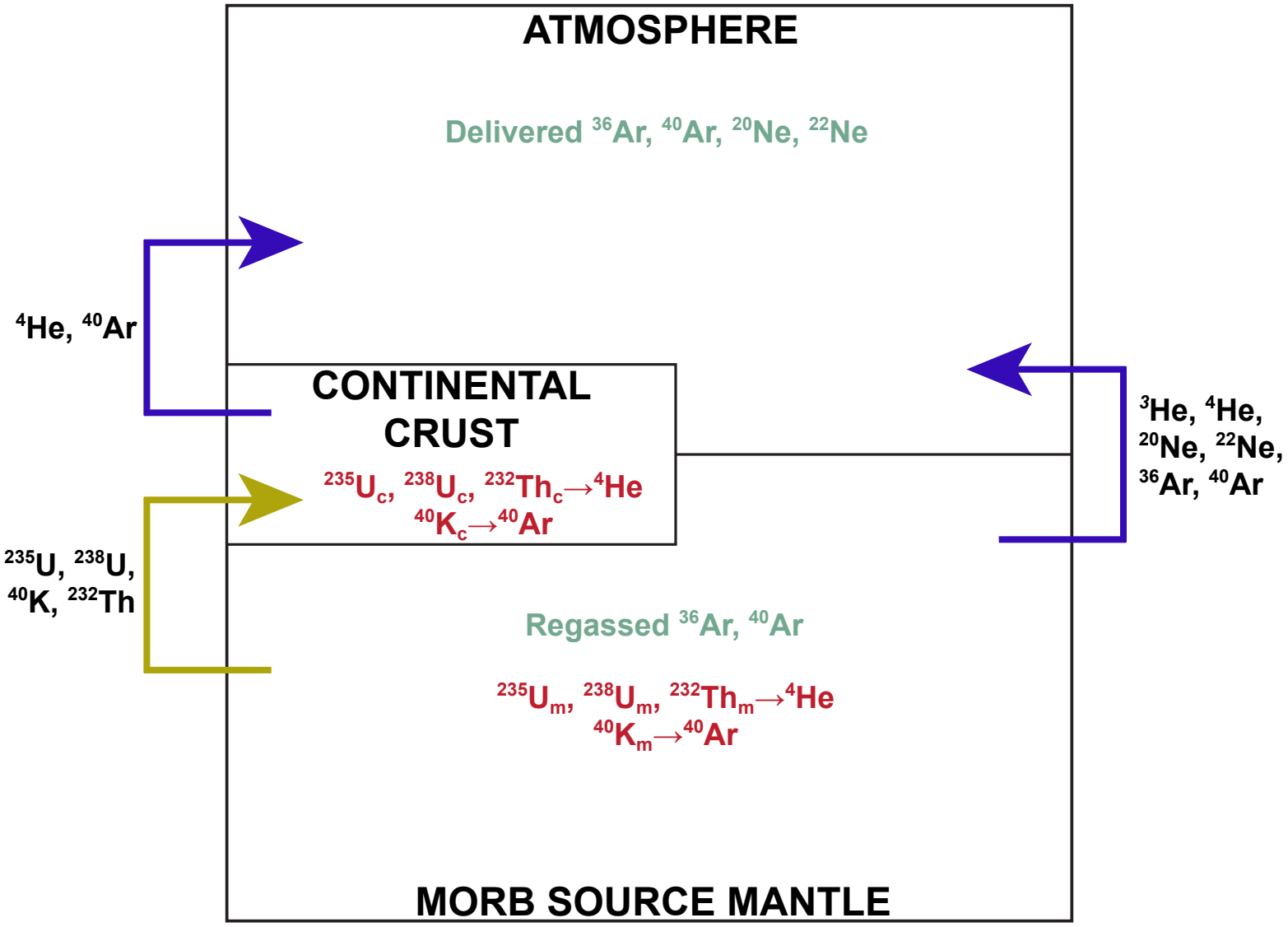
ATMOSPHERE
Delivered ^{36}Ar, ^{40}Ar, ^{20}Ne, ^{22}Ne
^{4}He, ^{40}Ar
CONTINENTAL CRUST
$^{235}U_c$, $^{238}U_c$, $^{232}Th_c \rightarrow {}^{4}He$
$^{40}K_c \rightarrow {}^{40}Ar$
^{3}He, ^{4}He, ^{20}Ne, ^{22}Ne, ^{36}Ar, ^{40}Ar
^{235}U, ^{238}U, ^{40}K, ^{232}Th
Regassed ^{36}Ar, ^{40}Ar
$^{235}U_m$, $^{238}U_m$, $^{232}Th_m \rightarrow {}^{4}He$
$^{40}K_m \rightarrow {}^{40}Ar$
MORB SOURCE MANTLE

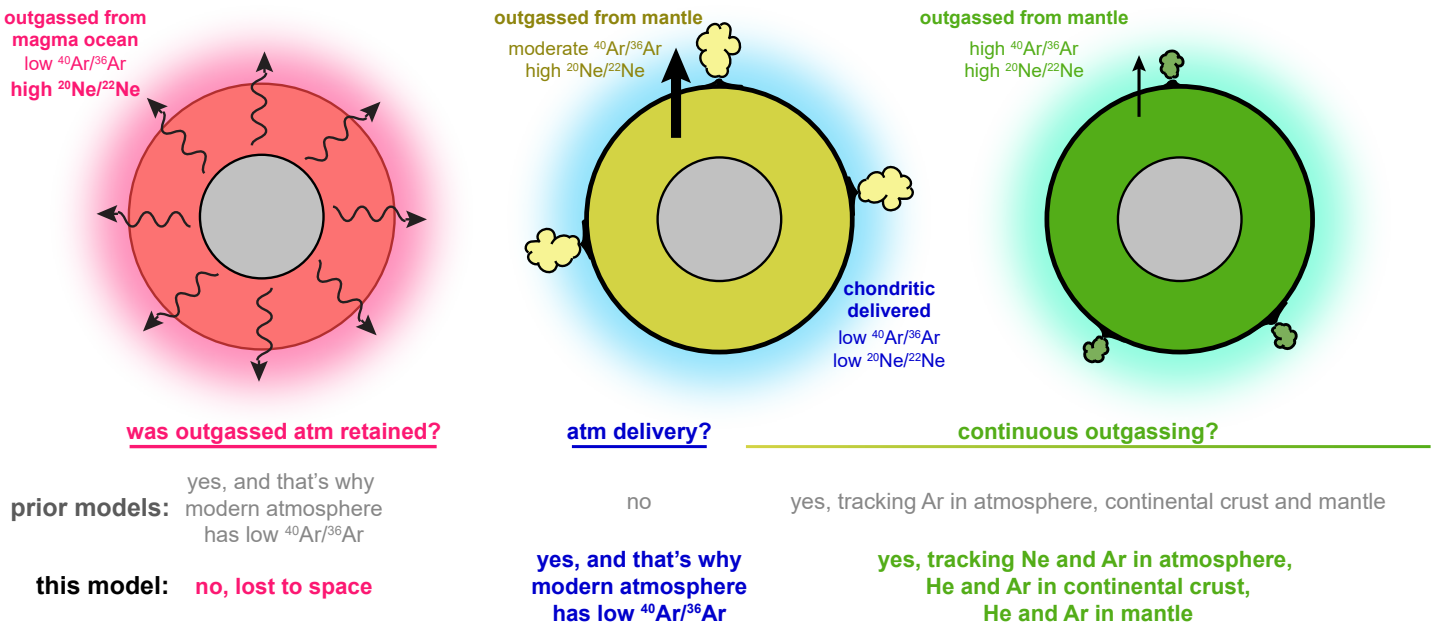
accretion
catastrophic outgassing
after giant impacts
after the last giant impact
impact degassing of late veneer
+
continuous outgassing
at a higher rate in the past
present
continuous outgassing
at the present-day rate
outgassed from
magma ocean
low 40Ar/36Ar
high 20Ne/22Ne
outgassed from mantle
moderate 40Ar/36Ar
high 20Ne/22Ne
chondritic
delivered
low 40Ar/36Ar
low 20Ne/22Ne
outgassed from mantle
high 40Ar/36Ar
high 20Ne/22Ne
was outgassed atm retained?
atm delivery?
continuous outgassing?
prior models:
yes, and that's why
modern atmosphere
has low 40Ar/36Ar
no
yes, tracking Ar in atmosphere, continental crust and mantle
this model:
no, lost to space
yes, and that's why
modern atmosphere
has low 40Ar/36Ar
yes, tracking Ne and Ar in atmosphere,
He and Ar in continental crust,
He and Ar in mantle

Figure 2

Figure 3

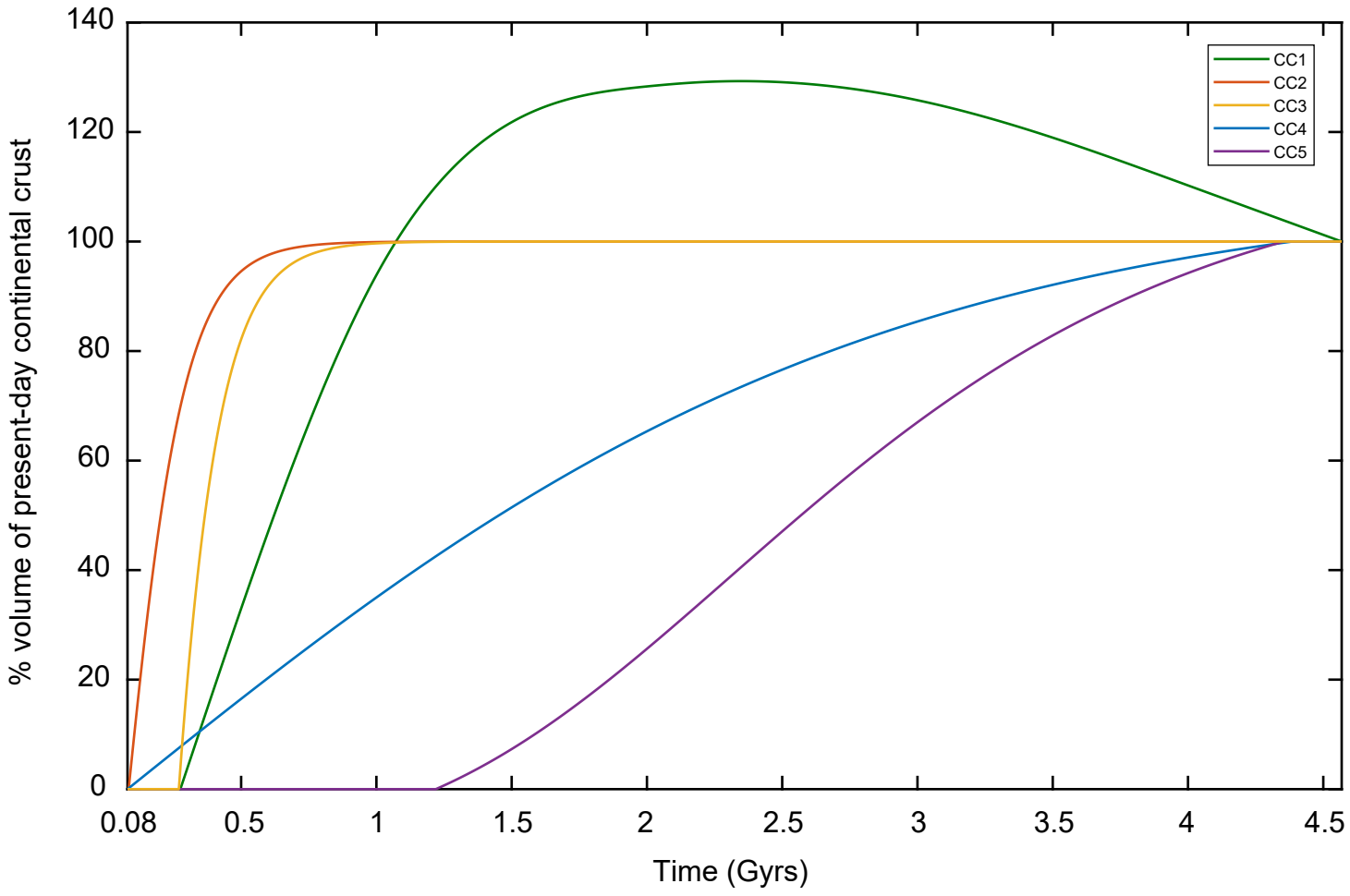
140
120
100
80
60
40
20
0
% volume of present-day continental crust
0.08
0.5
1
1.5
2
2.5
3
3.5
4
4.5
Time (Gyrs)
CC1
CC2
CC3
CC4
CC5

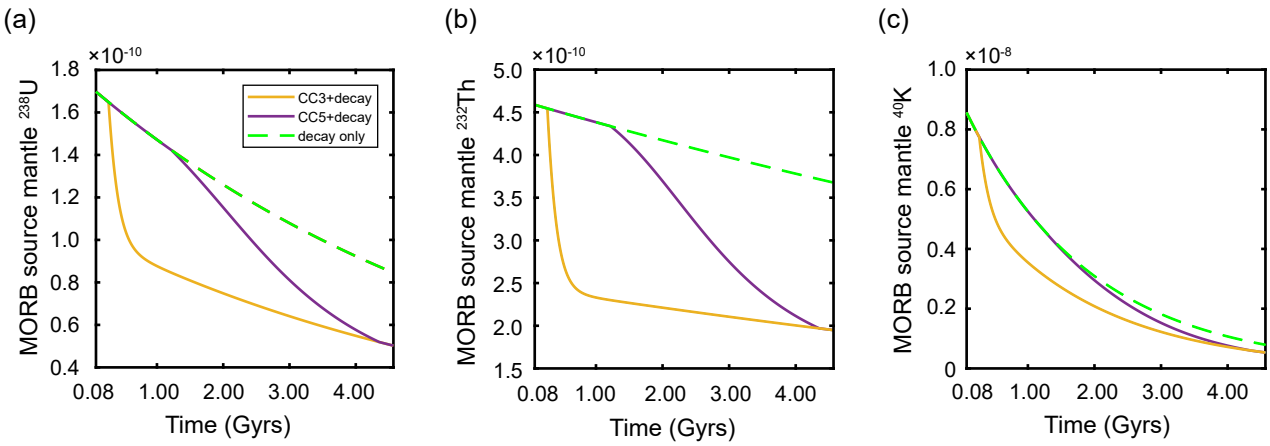
(a)
(b)
(c)
×10-10
×10-10
×10-8
MORB source mantle 238U
MORB source mantle 232Th
MORB source mantle 40K
CC3+decay
CC5+decay
decay only
Time (Gyrs)
Time (Gyrs)
Time (Gyrs)

Figure 4

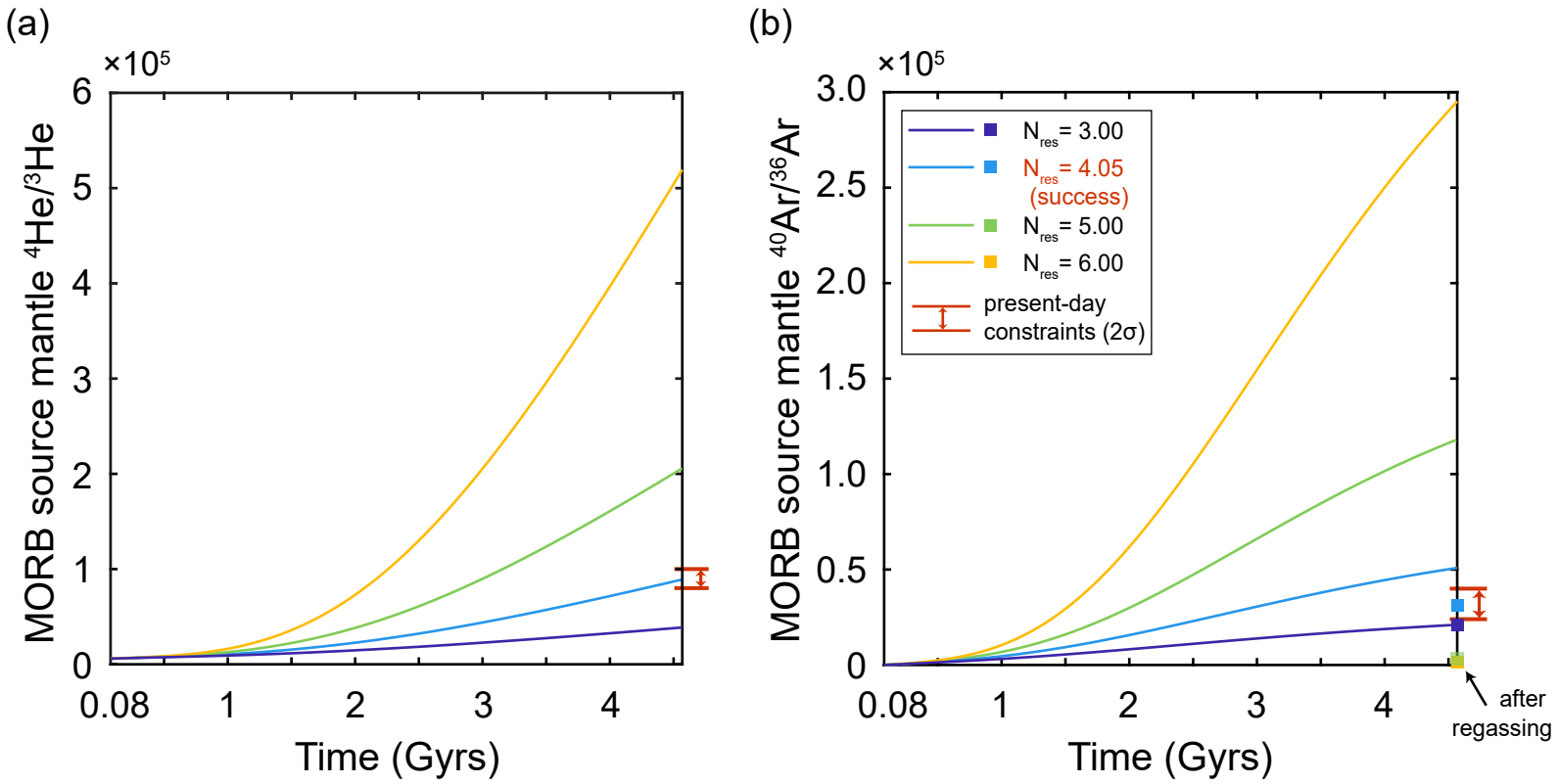
(a)
×10^5
MORB source mantle ^4He/^3He
Time (Gyrs)
(b)
×10^5
MORB source mantle ^40Ar/^36Ar
Time (Gyrs)
N_res = 3.00
N_res = 4.05 (success)
N_res = 5.00
N_res = 6.00
present-day constraints (2σ)
after regassing

Figure 5

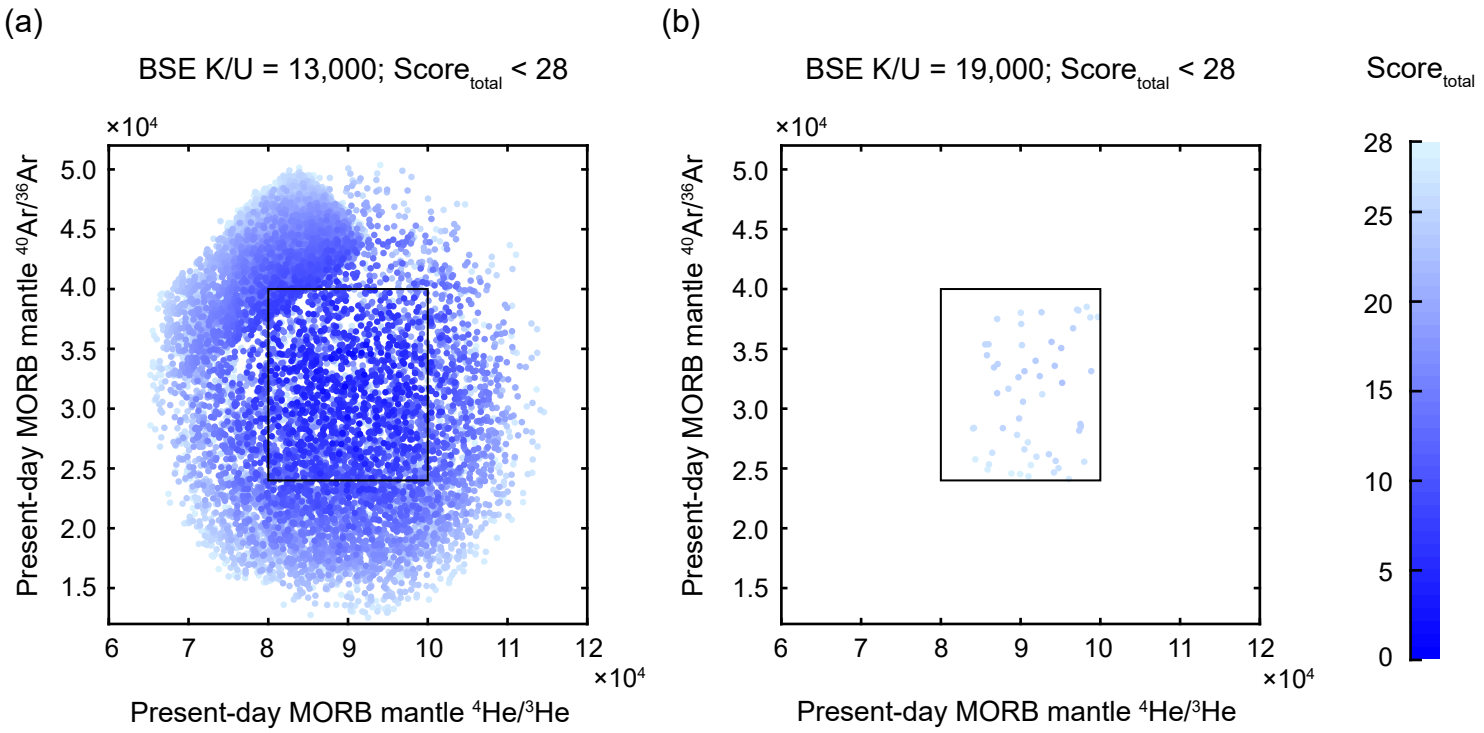
(a)
BSE K/U = 13,000; Score$_{total}$ < 28
×10^4
5.0
4.5
4.0
3.5
3.0
2.5
2.0
1.5
Present-day MORB mantle ^{40}Ar/^{36}Ar
6
7
8
9
10
11
12
×10^4
Present-day MORB mantle ^{4}He/^{3}He
(b)
BSE K/U = 19,000; Score$_{total}$ < 28
Score$_{total}$
28
25
20
15
10
5
0

Figure 6

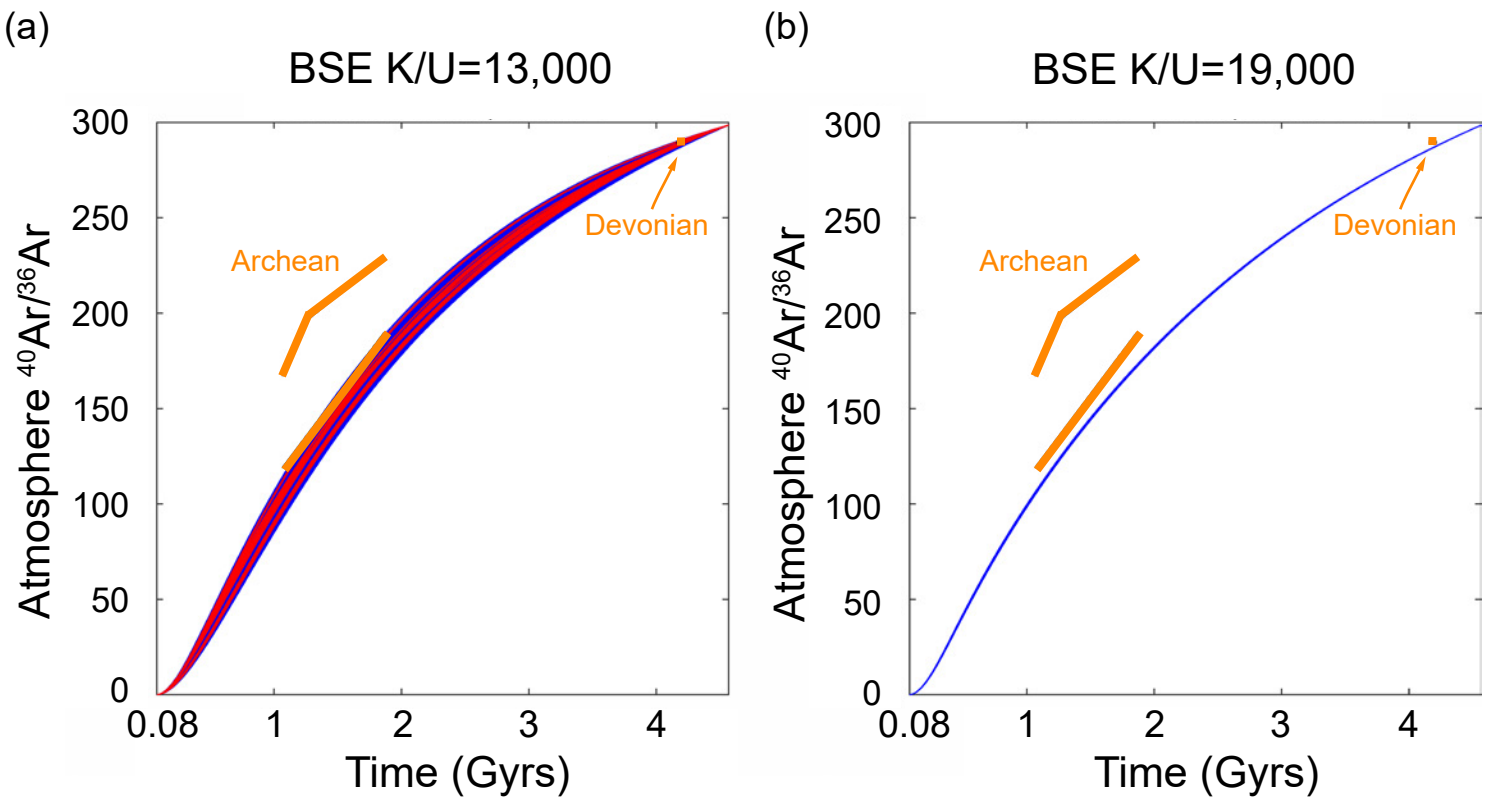
(a)
BSE K/U=13,000
Atmosphere $^{40}Ar/^{36}Ar$
300
250
200
150
100
50
0
0.08
1
2
3
4
Time (Gyrs)
Archean
Devonian
(b)
BSE K/U=19,000
Atmosphere $^{40}Ar/^{36}Ar$
300
250
200
150
100
50
0
0.08
1
2
3
4
Time (Gyrs)
Archean
Devonian

Figure 7

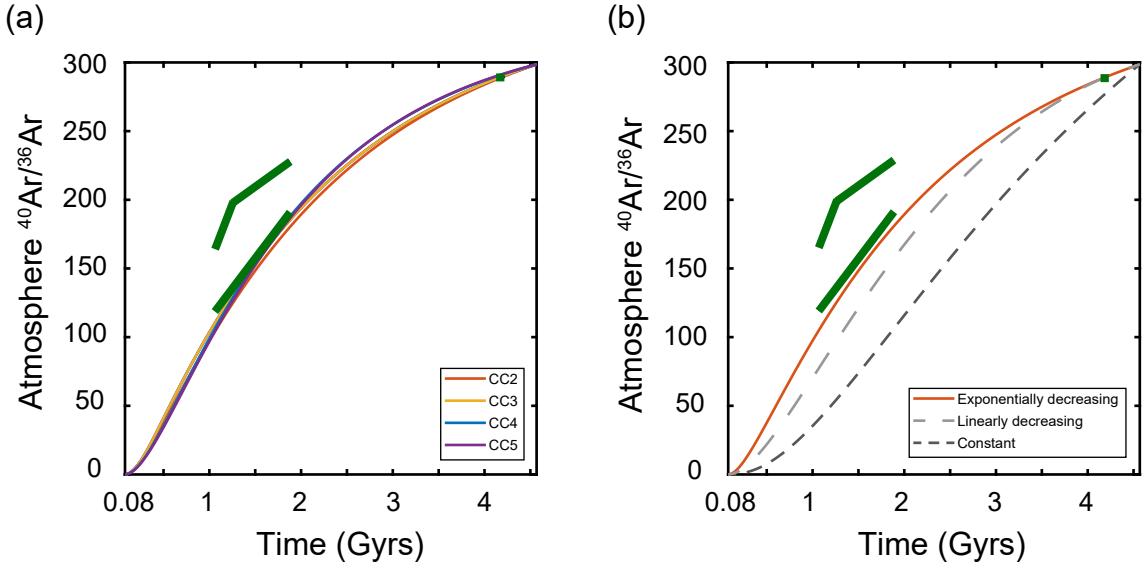
(a)
Atmosphere $^{40}Ar/^{36}Ar$
300
250
200
150
100
50
0
0.08
1
2
3
4
Time (Gyrs)
CC2
CC3
CC4
CC5
(b)
Atmosphere $^{40}Ar/^{36}Ar$
300
250
200
150
100
50
0
0.08
1
2
3
4
Time (Gyrs)
Exponentially decreasing
Linearly decreasing
Constant

Figure 8

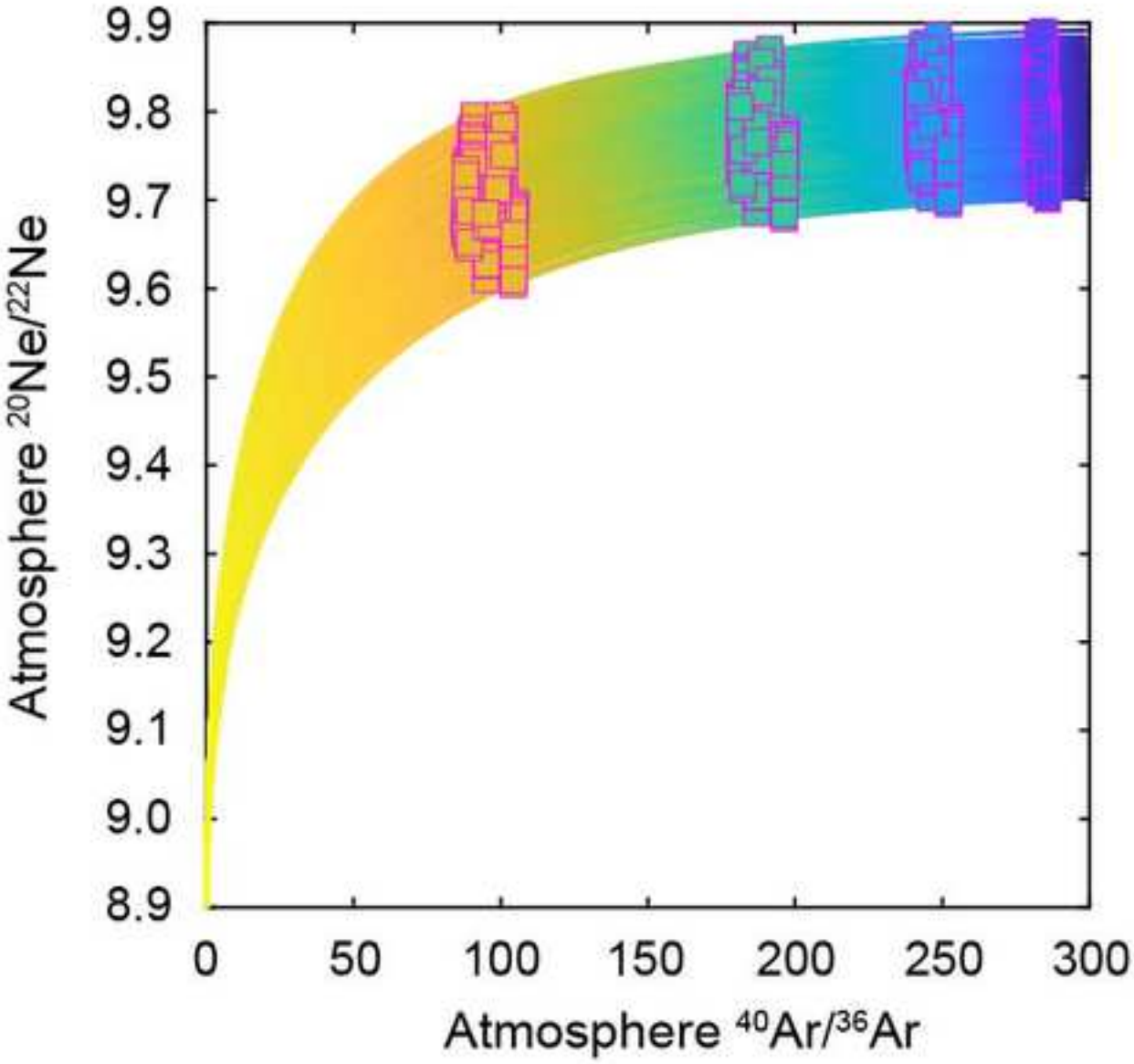
9.9
9.8
9.7
9.6
9.5
9.4
9.3
9.2
9.1
9.0
8.9
Atmosphere $^{20}Ne/^{22}Ne$
0
50
100
150
200
250
300
Atmosphere $^{40}Ar/^{36}Ar$

Figure 9

Supplementary Materials

For: Noble gas insights into early impact delivery and volcanic outgassing to Earth's atmosphere: a limited role for the continental crust

Xinmu J. Zhang, Guillaume Avice, Rita Parai

Contents:

Supplementary Text

Details of the numerical model setup:

The present-day MORB source mantle processing rate (*Qp*) is calculated based on the present-day processing rate at mid-ocean ridges of 21 km^3/yr (Crisp, 1984), assuming 10% partial melting producing mafic melt with a density of 2,900 kg/m^3 (Table S4, Equation 1). Given M_{res}, N_{res} and the present-day mantle processing rate, and assuming that the mantle processing rate decays exponentially over Earth history, the mantle processing rate is calculated as a function of time (Equation 2). For a given time step *dt* between time t_{last} and t_{now} (Equation 3), the accumulated mass of mantle processed (*dM*) is then computed (Equation 4).

The change in mass of the continental crust between time t_{now} and t_{last} (*dCC*) is calculated for each *CC* model assuming a constant density. To determine the net extraction of each incompatible lithophile elements U, Th and K from the MORB mantle to the continental crust, we calculate extraction constants *QU*, *QTh*, and *QK* for each given combination of M_{res} and *CC* model. For each combination of M_{res} and *CC* model, *QU* is the net extraction constant that satisfies U mass balance assuming the present-day U concentration of 1.3 ppm (Rudnick and Gao, 2003) in the continental crust reservoir ($M_{CC} = 2.28\times10^{25}$ g; McLennan and Taylor, 1982; Rudnick and Gao, 2003) was extracted from a bulk silicate Earth reservoir mass of M_{res} with a present-day U abundance of 20.3 ppb U (McCulloch and Bennett, 1994). The U depletion history of the MORB mantle thus depends on M_{res} and the *CC* model. We compute net extraction constants *QTh* and *QK* analogously, assuming the present-day continental crust Th and K concentration of 6.33 ppm and 1.63 wt% respectively (Rudnick and Gao, 2003). Within a given timestep, the change in U, Th, K

concentration in the MORB mantle due to net growth of the continental crust (accounting for both crustal growth and loss to erosion and subduction of sediments) are tracked (Equations 16-18).

Table S1. Model Parameters

a. Parameters explored with a Monte Carlo method							
Names	**Tested Range**	**Score$_{total}$ <7 Model Output Range (BSE K/U=9,000)**	**Score$_{total}$ <28 Model Output Range (BSE K/U=9,000)**	**Score$_{total}$ <7 Model Output Range (BSE K/U=13,000)**	**Score$_{total}$ <28 Model Output Range (BSE K/U=13,000)**	**Score$_{total}$ <28 Model Output Range (BSE K/U=19,000)**	**Description**
$^{3}He_{m,init}$	1.0×10^{9} to 1.0×10^{13} (atoms/gram)	1.3×10^{11} (atoms/gram)	1.0×10^{11} to 1.7×10^{11} (atoms/gram)	1.2×10^{11} to 2.1×10^{11} (atoms/gram)	1.0×10^{11} to 2.5×10^{11} (atoms/gram)	2.2×10^{11} to 2.7×10^{11} (atoms/gram)	The initial budget of mantle ^{3}He
$^{3}He_{m,init}/^{36}Ar_{m,init}$	1.12 to 1.43*	1.33 to 1.41	1.12 to 1.43	1.12 to 1.43	1.12 to 1.43	1.12 to 1.43	The initial mantle $^{3}He/^{36}Ar$ ratio
f	2.23×10^{-16} to 1.0 yr^{-1}	1.07×10^{-9} yr^{-1}	> 7.95×10^{-10} yr^{-1}	$1.98\times10^{-11}$$yr^{-1}$ to 2.05×10^{-9} yr^{-1}	full range	1.85×10^{-10} yr^{-1} to 1.89×10^{-10} yr^{-1}	The crustal degassing coefficient for Ar
b. Parameters describing mantle processing							
Names	**Tested Range**	**Score$_{total}$ <7 Model Output Range (BSE K/U=9,000)**	**Score$_{total}$ <28 Model Output Range (BSE K/U=9,000)**	**Score$_{total}$ <7 Model Output Range (BSE K/U=13,000)**	**Score$_{total}$ <28 Model Output Range (BSE K/U=13,000)**	**Score$_{total}$ <28 Model Output Range (BSE K/U=19,000)**	**Description**
N_{res}	2.00 to 15.0	4.05	3.75 to 4.50	3.90 to 4.80	3.60 to 5.10	5.85 to 6.00	The number of net mantle reservoir masses processed over the past 4.488

							billion years
M_{res}	2.0×10^{27} to 3.6×10^{27} grams, or 50% to 90% of the total mantle mass	*CC3* & M_{res}=90%	*CC2* & M_{res} = 82.5%; *CC3* & M_{res}= 90%; *CC4* & M_{res}= 90%	*CC2* & M_{res} = 90%; *CC3* & M_{res}=82.5% or 90%; *CC4* & M_{res}=62.5%; *CC5* & M_{res}=62.5%;	*CC2* & M_{res} = 82.5% or 90%; *CC3* & M_{res}=82.5% or 90%; *CC4* & M_{res}=62.5%; *CC5* & M_{res}=62.5%;	*CC3* & M_{res}=50%	The mass of the MORB mantle reservoir
CC models	$CC1\ to\ CC5$						Models of continental crust net volume growth as a function of time

*Calculated using $^{3}He/^{22}Ne$=10 and $^{36}Ar/^{22}Ne$ from 7 to 9 (see Section 2.1)

Table S2. Initial Noble Gas Budgets and Isotopic Compositions

Names	Values	Description
$^{3}He_{m,init}/\ ^{4}He_{m,init}$	120 R_A	The initial MORB source mantle $^{3}He/^{4}He$ ratio (Mahaffy et al., 1998)
$^{3}He_{m,init}/^{22}Ne_{m,init}$	10	The initial MORB source mantle $^{3}He/^{22}Ne$ ratio (Tucker and Mukhopadhyay, 2014)
$^{20}Ne_{m,init}/^{22}Ne_{m,init}$	12.6	The initial MORB source mantle $^{20}Ne/^{22}Ne$ ratio (Parai and Mukhopadhyay, 2021)
$^{20}Ne_{a,init}/^{22}Ne_{a,init} = {}^{20}Ne_{chon}/^{22}Ne_{chon}$	8.9	The initial atmospheric $^{20}Ne/^{22}Ne$ ratio (Williams and Mukhopadhyay, 2019; Mazor et al., 1970)
$^{36}Ar_{m,init}/^{22}Ne_{m,init}$	7 to 9	The initial MORB source mantle $^{36}Ar/^{22}Ne$ ratio (from the present-day depleted mantle values; Marty, 2012)
$^{36}Ar_{a,init}/^{22}Ne_{a,init} = {}^{36}Ar_{chon}/^{22}Ne_{chon}$	20	The initial atmospheric $^{36}Ar/^{22}Ne$ ratio (based on CI chondrites; Williams and Mukhopadhyay, 2019; Mazor et al., 1970)
$^{40}Ar_{a,init}/^{36}Ar_{a,init} = {}^{40}Ar_{chon}/^{36}Ar_{chon}$	0.1	The initial MORB source mantle $^{40}Ar/^{36}Ar$ ratio (upper limit estimate of chondritic dominated by Q component; Ott, 2002)
$^{36}Ar_{a,init}$	0	The initial atmospheric ^{36}Ar content
$^{40}Ar_{a,init}$	0	The initial atmospheric ^{40}Ar content

Table S3. Radioactive Decay Constants

Radioactive species	Decay constant λ
^{235}U	9.8496×10^{-10}
^{238}U	1.5514×10^{-10}
^{232}Th	4.9334×10^{-11}
^{40}K*	5.3050×10^{-10}

*The branch ratio of the radioactive decay $^{40}K \rightarrow {}^{40}Ar$ is 0.10482.

Equations

Mantle processing:	
$Q_p = 21 \times 2.9 \times 10^{15} \div 10\% = 6.09 \times 10^{17}\ (g/yr)$	Eq. 1
$Q(t) = Q_p e^{\alpha(T-t)}$	Eq. 2
$dt = t_{now} - t_{last}$	Eq. 3
$dM = Q_p * \frac{T}{\alpha} * (e^{\frac{\alpha t_{last}}{T}} - e^{\frac{\alpha t_{now}}{T}})$	Eq. 4
Mantle species with time series:	
$^{235}U_{m,now} = {}^{235}U_{m,last} e^{-\lambda_{235} dt} - dUCC \times ratio_{235238}$	Eq. 5
$^{238}U_{m,now} = {}^{238}U_{m,last} e^{-\lambda_{238} dt} - dUCC \times (1 - ratio_{235238})$	Eq. 6
$^{232}Th_{m,now} = {}^{232}Th_{m,last} e^{-\lambda_{232} dt} - dThCC$	Eq. 7
$^{40}K_{m,now} = {}^{40}K_{m,last} e^{-\lambda_{40} dt} - dKCC$	Eq. 8
$^{3}He_{m,now} = {}^{3}He_{m,last} \times (1 - \frac{dM}{M_{res}})$	Eq. 9
$^{4}He_{m,now} = \left[{}^{4}He_{m,last} + 8 \times {}^{238}U_{m,last}\left(1 - e^{-\lambda_{238} dt}\right) + 7 \times {}^{235}U_{m,last}\left(1 - e^{-\lambda_{235} dt}\right) + 6 \times {}^{232}Th_{m,last}\left(1 - e^{-\lambda_{232} dt}\right) \right] \times \left(1 - \frac{dM}{M_{res}}\right)$	Eq. 10

$^{20}Ne_{m,now} = {}^{20}Ne_{m,last} \times (1 - \frac{dM}{M_{res}})$	Eq. 11
$^{22}Ne_{m,now} = {}^{22}Ne_{m,last} \times (1 - \frac{dM}{M_{res}})$	Eq. 12
$^{36}Ar_{m,now} = {}^{36}Ar_{m,last} \times (1 - \frac{dM}{M_{res}})$	Eq. 13
$^{40}Ar_{m,now} = \left[{}^{40}Ar_{m,last} + {}^{40}K_{m,last}\left(1 - e^{-\lambda_{40}dt}\right) \times ktoar\right] \times \left(1 - \frac{dM}{M_{res}}\right)$	Eq. 14
Continental crust:	
$m_{c,now} = m_{c,last} + dCC \times m_{c,T}$	Eq. 15
$dUCC = dCC \times QU$	Eq. 16
$dKCC = dCC \times QK$	Eq. 17
$dThCC = dCC \times QTh$	Eq. 18
$^{235}U_{c,now} = \frac{(^{235}U_{c,last} \times m_{c,last} + dUCC \times M_{res} \times ratio_{235vstotalU})e^{-\lambda_{235}dt}}{m_{c,now}}$	Eq. 19
$^{238}U_{c,now} = \frac{[^{238}U_{c,last} \times m_{c,last} + dUCC \times M_{res} \times (1 - ratio_{235vstotalU})]e^{-\lambda_{238}dt}}{m_{c,now}}$	Eq. 20
$^{232}Th_{c,now} = \frac{(^{232}Th_{c,last} \times m_{c,last} + dThCC \times M_{res})e^{-\lambda_{232}dt}}{m_{c,now}}$	Eq. 21

$^{40}K_{c,now} = \frac{(^{40}K_{c,last} \times m_{c,last} + dKCC \times M_{res})e^{-\lambda_{40}dt}}{m_{c,now}}$	Eq. 22
$^{40}Ar_{c,now} = [^{40}Ar_{c,last} + {}^{40}K_{c,last}(1 - e^{-\lambda_{40}dt}) \times ktoar \times m_{c,last}] \times (1 - f)$	Eq. 23
<u>Atmosphere:</u>	
$^{20}Ne_{a,now} = {}^{20}Ne_{a,last} + {}^{20}Ne_{m,last} \times dM$	Eq. 24
$^{22}Ne_{a,now} = {}^{22}Ne_{a,last} + {}^{22}Ne_{m,last} \times dM$	Eq. 25
$^{36}Ar_{a,now} = {}^{36}Ar_{a,last} + {}^{36}Ar_{m,last} \times dM$	Eq. 26
$^{40}Ar_{a,now} = {}^{40}Ar_{a,last} + [{}^{40}Ar_{m,last} + {}^{40}K_{m,last}(1 - e^{-\lambda_{40}dt}) \times ktoar] \times dM + [{}^{40}K_{c,last}(1 - e^{-\lambda_{40}dt}) \times ktoar \times m_{c,last}] \times f$	Eq. 27
<u>Net chondritic delivery of atmospheric Ar and Ne:</u>	
$^{36}Ar_{a,delivery} = \left[{}^{40}Ar_{a,end} - {}^{36}Ar_{a,end} \times \left(\frac{^{40}Ar_{a,today}}{^{36}Ar_{a,today}}\right)\right] \div \left[\left(\frac{^{40}Ar_{a,today}}{^{36}Ar_{a,today}}\right) - \left(\frac{^{40}Ar_{chon}}{^{36}Ar_{chon}}\right)\right]$	Eq. 28
$^{40}Ar_{a,delivery} = {}^{36}Ar_{a,delivery} \times \left(\frac{^{40}Ar_{chon}}{^{36}Ar_{chon}}\right)$	Eq. 29
$^{22}Ne_{a,delivery} = {}^{36}Ar_{a,delivery} \times \left(\frac{^{22}Ne_{chon}}{^{36}Ar_{chon}}\right)$	Eq. 30

$^{20}\mathrm{Ne}_{\mathrm{a,delivery}} = {}^{22}\mathrm{Ne}_{\mathrm{a,delivery}} \times \left(\frac{^{20}\mathrm{Ne}_{\mathrm{chon}}}{^{22}\mathrm{Ne}_{\mathrm{chon}}} \right)$	Eq. 31
<u>Regassing of excess atmospheric Ar (if any) to the mantle:</u>	
$^{40}\mathrm{Ar}_{\mathrm{regassed\ to\ mantle}} = {}^{40}\mathrm{Ar}_{\mathrm{a,end}} - {}^{40}\mathrm{Ar}_{\mathrm{a,today}}$	Eq. 32
$^{36}\mathrm{Ar}_{\mathrm{regassed\ to\ mantle}} = {}^{36}\mathrm{Ar}_{\mathrm{a,end}} - {}^{40}\mathrm{Ar}_{\mathrm{a,today}} \times \left({}^{40}\mathrm{Ar}_{\mathrm{a,today}} / {}^{36}\mathrm{Ar}_{\mathrm{a,today}} \right)$	Eq. 33
$^{40}\mathrm{Ar}_{\mathrm{m,end,after\ regassing}} = {}^{40}\mathrm{Ar}_{\mathrm{m,end}} + {}^{40}\mathrm{Ar}_{\mathrm{regassed\ to\ mantle}}$	Eq. 34
$^{36}\mathrm{Ar}_{\mathrm{m,end,after\ regassing}} = {}^{36}\mathrm{Ar}_{\mathrm{m,end}} + {}^{36}\mathrm{Ar}_{\mathrm{regassed\ to\ mantle}}$	Eq. 35
<u>Performance score calculations:</u>	
$Score_{m,He} = \left[\frac{({}^{4}He_{\mathrm{m,end}} / {}^{3}He_{\mathrm{m,end}}) - 90000}{5000} \right]^2$	Eq. 36
$Score_{a,Ne} = \left[\frac{(^{20}Ne_{a,\mathrm{end}} / ^{22}Ne_{a,\mathrm{end}}) - 9.8}{0.04} \right]^2$	Eq. 37
$Score_{a,Ne,today} = \left[\frac{^{22}Ne_{a,\mathrm{end}} - 2.9925 \times 10^{14}}{5 \times 10^{13}} \right]^2$	Eq. 38
$Score_{a,Ar,today} = \left[\frac{^{40}Ar_{a,\mathrm{end}} - 1.6548 \times 10^{18}}{1.6548 \times 10^{16}} \right]^2$	Eq. 39

$Score_{m,Ar} = \left[\frac{(^{40}Ar_{m,\text{end,after regassing}}/^{36}Ar_{\text{m,end,after regassing}}) - 32000}{4000}\right]^2$	Eq. 40
$Score_{a,Ar,Archean} = \min\left(\left[\frac{(^{40}Ar_{a,\text{Archean}}/^{36}Ar_{a,\text{Archean}}) - \left(\frac{^{40}Ar_a}{^{36}Ar_a}\right)_{Archean,mean}}{32}\right]^2\right)$	Eq. 41
$Score_{a,Ar,Devonian} = \min\left(\left[\frac{(^{40}Ar_{a,\text{Devonian}}/^{36}Ar_{a,\text{Devonian}}) - \left(\frac{^{40}Ar_a}{^{36}Ar_a}\right)_{Devonian,mean}}{0.4}\right]^2\right)$	Eq. 42
$Score_{total} = Score_{m,He} + Score_{a,Ne} + Score_{a,Ne,today} + Score_{a,Ar,today} + Score_{m,Ar} + Score_{a,Ar,Archean} + Score_{a,Ar,Devonian}$	Eq. 43

*32 is the average uncertainty computed for Pujol et al.'s constraint over the 2.7 Ga to 3.5 Ga range. The minimum residual in the time range is used for the score.

**0.4 is the average uncertainty computed for Stuart et al.'s constraint in the 380 ± 30 Ma range. The minimum residual in the time range is used for the score.

Table S5. Noble Gas Model Constraints

Observations		Values*	Description
$^{4}He_{m,today}/\ ^{3}He_{m,today}$		90,000 ± 10,000	The present-day MORB source mantle $^{4}He/^{3}He$ ratio (Graham, 2002)
$^{20}Ne_{a,today}/^{22}Ne_{a,today}$		9.8 ± 0.16	The present-day atmospheric $^{20}Ne/^{22}Ne$ ratio (Eberhardt et al., 1965)
$^{22}Ne_{a,today}$		2.9925×10^{14} moles	The present-day atmospheric ^{22}Ne mole abundance (Eberhardt et al., 1965)
$^{40}Ar_{a,today}$		1.6548×10^{18} moles	The present-day atmospheric ^{40}Ar mole abundance (Porcelli and Ballentine, 2002)
$^{40}Ar_{a,today}/^{36}Ar_{a,today}$		298.6 (fixed in model setup)	The present-day atmospheric $^{40}Ar/^{36}Ar$ ratio (Lee et al., 2006)
$^{40}Ar_{m,today}/^{36}Ar_{m,today}$		32,000 ± 8,000	The present-day MORB source mantle $^{40}Ar/^{36}Ar$ ratio (Parai et al., 2012; Parai and Mukhopadhyay, 2021)
$\frac{^{40}Ar_{a,Archean}}{^{36}Ar_{a,Archean}}$	3.5 Ga	119 to 167	Archean atmospheric $^{40}Ar/^{36}Ar$ ratios (with age uncertainties; Pujol et al., 2013)
	3.0 Ga	137 to 200	
	2.7 Ga	190 to 232	
$^{40}Ar_{a,Devonian}/^{36}Ar_{a,Devonian}$		289.5 ± 0.4	Devonian atmospheric $^{40}Ar/^{36}Ar$ ratios (380 ± 30 Ma, Cadogan, 1977; Stuart et al., 2016)

*Errors are 2σ.

Supplementary Figures:

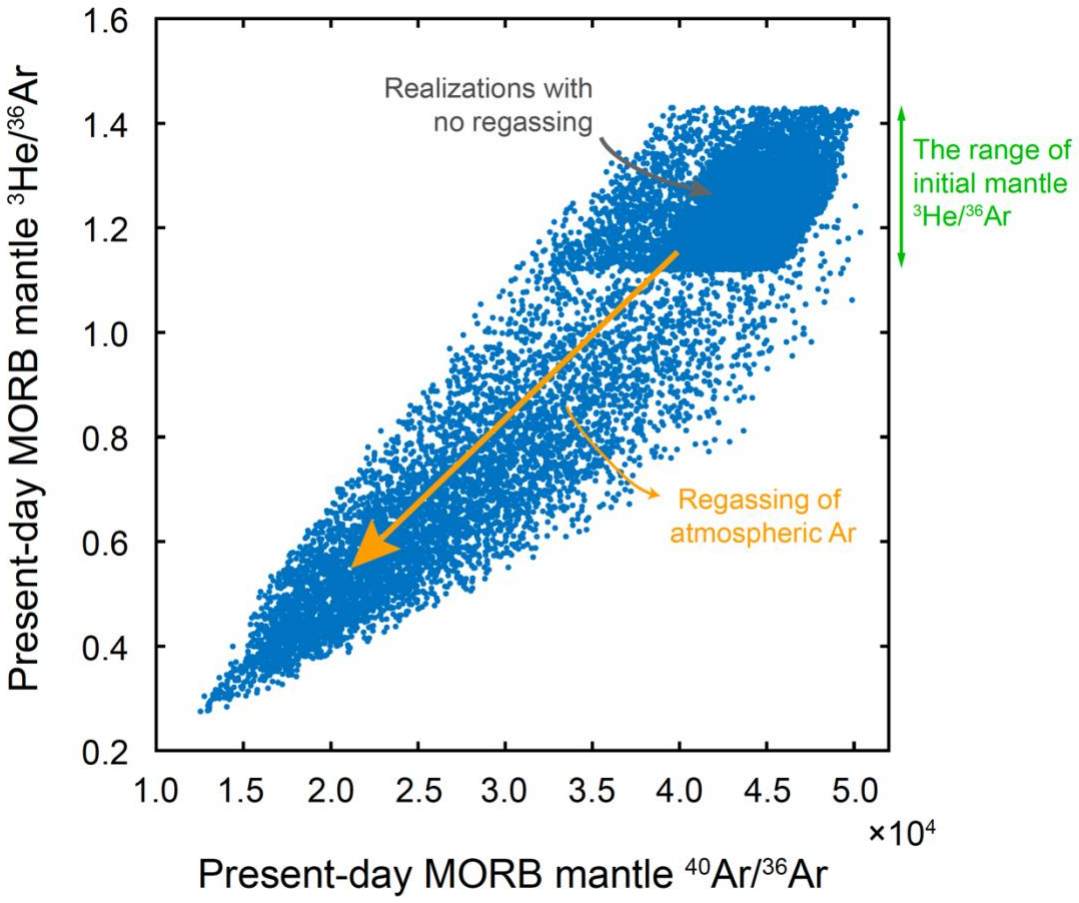

Figure S1. Present-day mantle $^{3}He/^{36}Ar$ and $^{40}Ar/^{36}Ar$ including regassed Ar for successful ($Score_{total}$<28) model realizations with BSE K/U=13,000. The initial mantle $^{3}He/^{36}Ar$ ratio is a model input parameter with an allowed range from 1.12 to 1.43 (Tables 1 and S1). Any addition of regassed atmospheric Ar with $^{40}Ar/^{36}Ar$ ratio of 298.6 would decrease the mantle $^{3}He/^{36}Ar$ ratio as well as the mantle $^{40}Ar/^{36}Ar$ ratio, as shown by the orange arrow. The cluster of dots in the upper right corner are within the range of the initial mantle $^{3}He/^{36}Ar$ ratio; these model realizations yield atmospheric Ar abundances lower than (but within tolerance of) the observed atmospheric Ar abundance, and thus do not invoke atmospheric Ar regassing. Some successful model realizations can be achieved without invoking Ar regassing, but other successful model realizations require Ar regassing. The model realizations with no regassing correspond to the model realization cluster with present-day mantle $^{40}Ar/^{36}Ar$ of ~40,000 in Figure 6a.

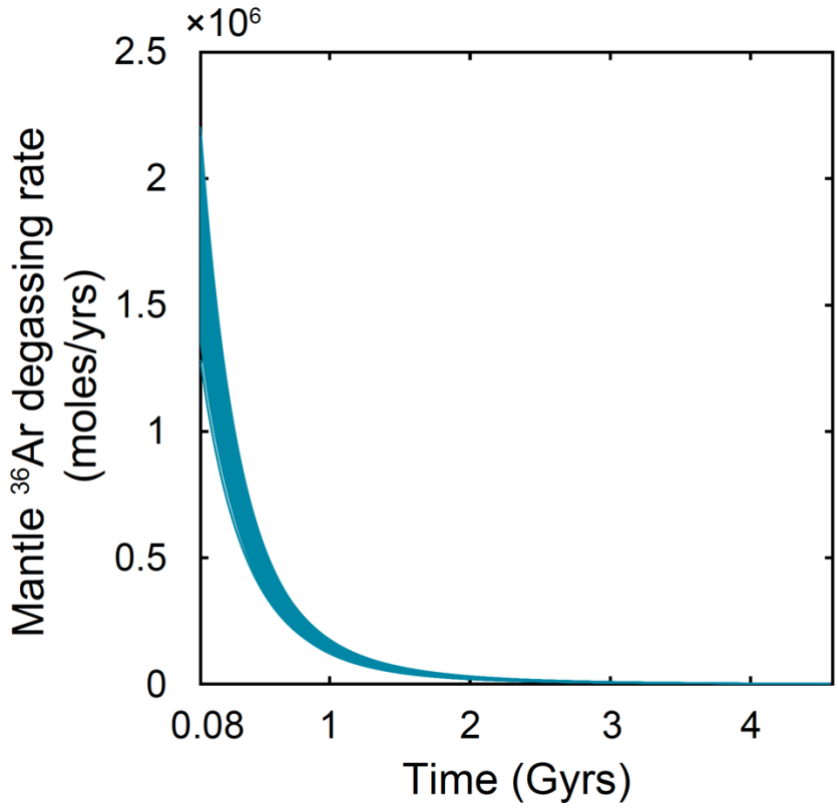

Figure S2. Mantle degassing flux for ^{36}Ar for successful (Score$_{total}$<7) model realizations with BSE K/U=13,000. Starting at the end of accretion, the degassing rate of ^{36}Ar (as well as other stable, non-radiogenic noble gas nuclides) decays near-exponentially over time. The range in the initial ^{36}Ar degassing flux reflects the range of initial ^{36}Ar abundances, reservoir mass and total degree of mantle melting.

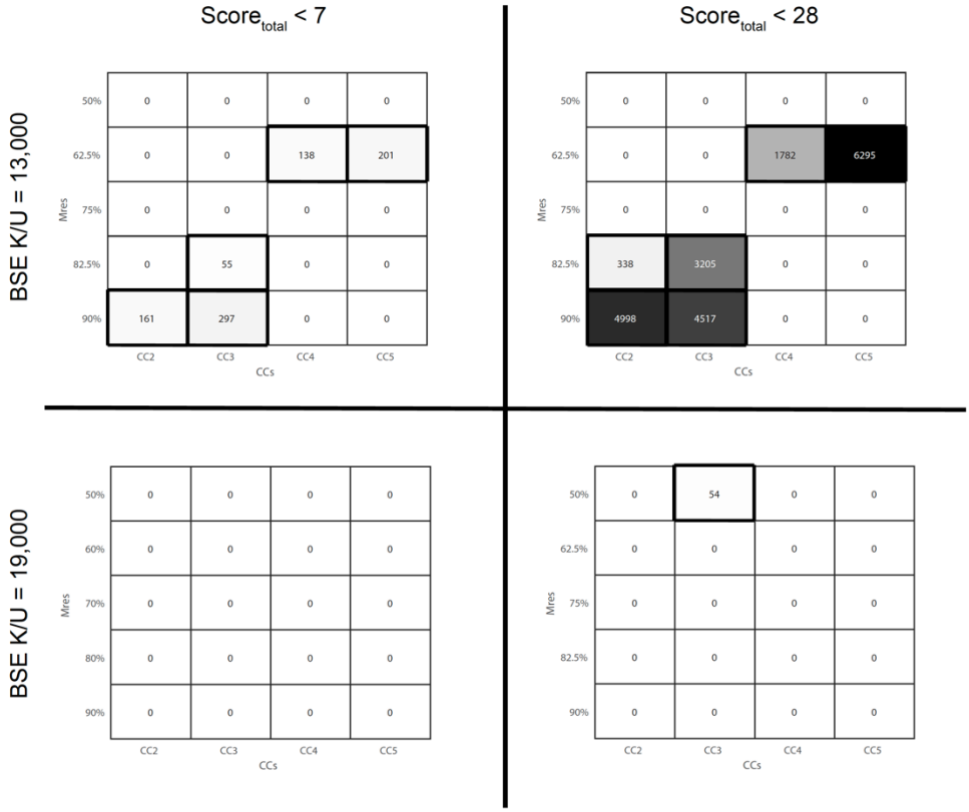

Figure S3. The number of successful model realizations for each combination of parameters. The color map shows the number of successful model realizations with $Score_{total}$<28 and $Score_{total}$<7 generated by different combinations M_{res} and net continental crust growth model given a total of 100,000 model simulations for each initial BSE K/U ratio. Combinations that provide model successes are shown with bold borders. Darker colors correspond to larger numbers of model successes with this specific parameter combination. If combined with smaller MORB source mantle masses, models with later onset of net continental crust growth (*CC4* & *CC5*) can provide successful model solutions that are able to account for mantle and atmospheric without invoking outgassing of the whole mantle. However, outgassing from a plume mantle with ~40% of total mantle mass is likely to be significant, so the successful model realizations found with late onsets of continental crust growth may not be realistic. Compared to the high BSE K/U scenario, the low BSE K/U scenario generates more model successes in each score category. Successful model realizations with a lower BSE K/U ratio of 13,000 generally have lower sensitivity and requirements on other model parameters. Therefore, more combinations of M_{res} and continental crust growth scenario are able to provide model success compared to the high BSE K/U case.

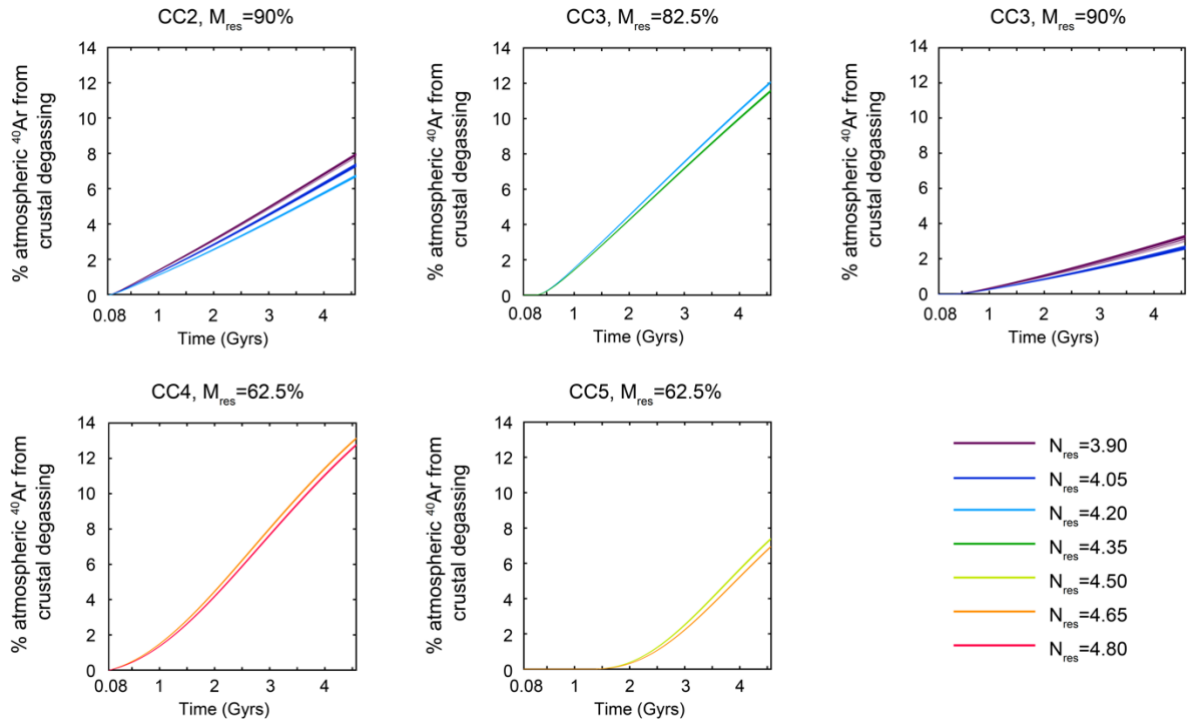

Figure S4. Cumulative contribution of atmospheric ^{40}Ar from crustal outgassing for Score$_{total}$<7 model realizations. Each subplot shows the percentage of total atmospheric ^{40}Ar that was produced in the continental crust and degassed to the atmosphere via crustal processes over time, with a specified set of *CC* models and *Mres* combinations, as well as different *Nres* that together generated model successes with Score$_{total}$<7. Among all successful model realizations, crustal degassing contributes at most 13% of the present-day atmospheric ^{40}Ar, broadly consistent with the estimate from Sarda et al. (1985). Earlier onset of net continental crust growth generally leads to a higher proportion of atmospheric ^{40}Ar from crustal outgassing, due to the transport of ^{40}K into the growing continental crust and more rapid ^{40}K decay early in Earth's history. Smaller *Mres* translates to less ^{40}K in the depleted mantle and less mantle ^{40}Ar ingrowth, such that crustal degassing provides a higher proportion of present-day atmospheric ^{40}Ar (panel d). *Nres* has a limited effect on the contribution of ^{40}Ar from crustal degassing. A very small proportion of atmospheric ^{40}Ar is from delivery, and most atmospheric ^{40}Ar is from mantle outgassing.

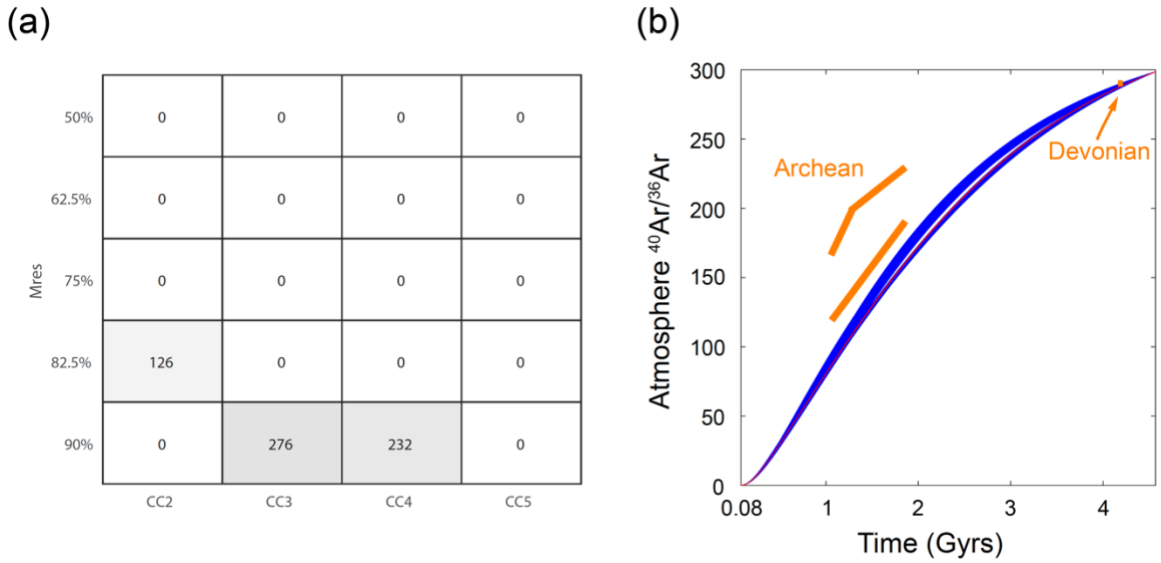

Figure S5. Successful model realizations for BSE K/U=9,000. (a) The number of model realizations with $Score_{total}$ <28 for each combination of model parameters out of 5×10^4 model runs (note that this is half of the total number of model runs performed in each Figure S3 panels). Successful model realizations of BSE K/U=9,000 are more sensitive to other model parameters compared to the BSE K/U estimates of 13,000 (Figure S3). (b) Atmospheric $^{40}Ar/^{36}Ar$ isotopic compositions over time for successful model realizations of BSE K/U=9,000. Blue and red curves are model realizations with $Score_{total}$<28 and $Score_{total}$<7 respectively. A lower BSE K/U of 9,000 leads to a decreased amount of mantle ^{40}Ar production and a slightly lower Archean atmospheric $^{40}Ar/^{36}Ar$ ratio than the observational constraint (and lower than found in model realizations using a BSE K/U of 13,000; Figure 7a).

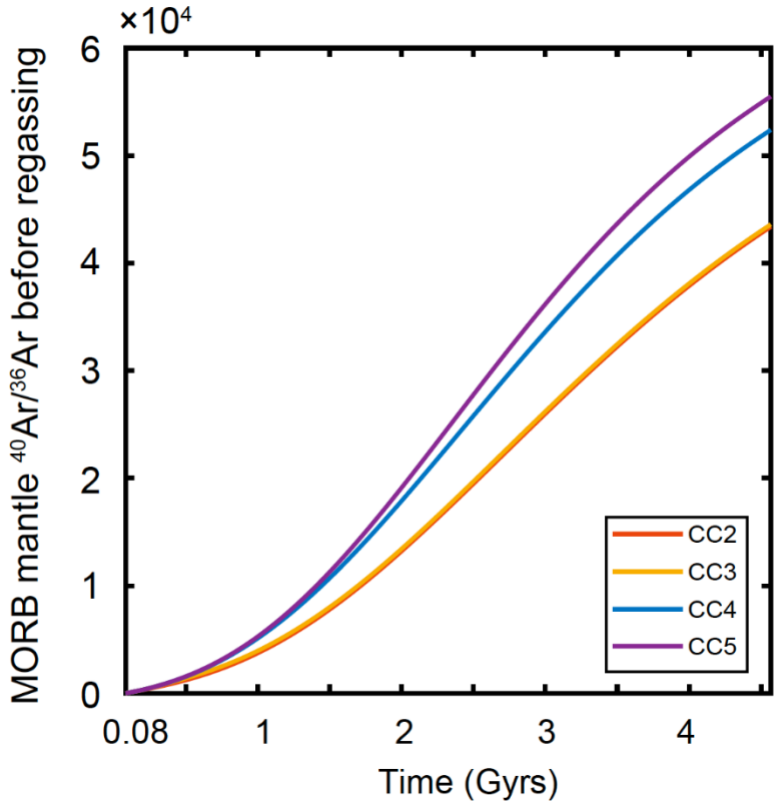

Figure S6. MORB source mantle $^{40}Ar/^{36}Ar$ ratio time evolution curves generated by varying *CC* model only. Curves correspond to the model realizations shown in Figure 8a. Early net continental crust growth can transport more ^{40}K from the mantle to the crust compared to scenarios with late net crustal growth, leading to slightly lower mantle $^{40}Ar/^{36}Ar$ ratios (*CC2* and *CC3* in red and yellow, overlapping). However, compared to different mantle outgassing rates (parameterized by N_{res}) that generate large variations in mantle Ar isotopic compositions over time (Figure 5b), differences in continental crust growth introduce small variations in mantle $^{40}Ar/^{36}Ar$ compared to the atmospheric composition, explaining the limited sensitivity of atmospheric $^{40}Ar/^{36}Ar$ ratio regarding *CC* models (Figure 8a).

References

Cadogan, P.H., 1977. Palaeoatmospheric argon in Rhynie chert. Nature 1977 268:5615 268, 38–41. https://doi.org/10.1038/268038a0

Crisp, J.A., 1984. Rates of magma emplacement and volcanic output. J. Volcanol. Geotherm. Res. https://doi.org/10.1016/0377-0273(84)90039-8

Eberhardt, P., Eugster, O. and Marti, K., 1965. A redetermination of the isotopic composition of atmospheric neon. Zeitschrift für Naturforschung A, 20(4), 623-624

Graham, D.W., 2002. Noble gas isotope geochemistry of mid-ocean ridge and ocean island basalts: Characterization of mantle source reservoirs. Rev. Mineral. Geochemistry 47, 247–317. https://doi.org/10.2138/rmg.2002.47.8

Lee, J.-Y., Marti, K., Severinghaus, J.P., Kawamura, K., Yoo, H.-S., Lee, J.B., Kim, J.S., 2006. A redetermination of the isotopic abundances of atmospheric Ar. Geochim. Cosmochim. Acta 70, 4507–4512. https://doi.org/10.1016/j.gca.2006.06.1563

Mahaffy, P.R., Donahue, T.M., Atreya, S.K., Owen, T.C., Niemann, H.B., 1998. Galileo probe measurements of D/H and 3He/4He in Jupiter's atmosphere. Space Sci. Rev. https://doi.org/10.1023/a:1005091806594

Marty, B., 2012. The origins and concentrations of water, carbon, nitrogen and noble gases on Earth. Earth Planet. Sci. Lett 313–314, 56–66. https://doi.org/10.1016/j.epsl.2011.10.040

Mazor, E., Heymann, D., Anders, E., 1970. Noble gases in carbonaceous chondrites. Geochim. Cosmochim. Acta. https://doi.org/10.1016/0016-7037(70)90031-1

McCulloch, M.T., Bennett, V.C., 1994. Progressive growth of the Earth's continental crust and depleted mantle: Geochemical constraints. Geochim. Cosmochim. Acta 58, 4717–4738. https://doi.org/10.1016/0016-7037(94)90203-8

McLennan, S.M., Taylor, S.R., 1982. Geochemical constraints on the growth of the continental crust. J. Geol. https://doi.org/10.1086/628690

Ott, U., 2002. Noble gases in meteorites - Trapped components. Rev. Mineral. Geochemistry 47, 71–100. https://doi.org/10.2138/rmg.2002.47.3

Parai, R., Mukhopadhyay, S., 2021. Heavy noble gas signatures of the North Atlantic Popping Rock 2ΠD43: Implications for mantle noble gas heterogeneity. Geochim. Cosmochim. Acta 294, 89–105. https://doi.org/10.1016/J.GCA.2020.11.011

Parai, R., Mukhopadhyay, S., Standish, J.J., 2012. Heterogeneous upper mantle Ne, Ar and Xe isotopic compositions and a possible Dupal noble gas signature recorded in basalts from the Southwest Indian Ridge. Earth Planet Sci Lett. 359–360, 227–239. https://doi.org/10.1016/J.EPSL.2012.10.017

Porcelli, D., Ballentine, C. J., 2002. Models for Distribution of Terrestrial Noble Gases and Evolution of the Atmosphere. Reviews in Mineralogy and Geochemistry 47 (1): 411–480. doi: https://doi.org/10.2138/rmg.2002.47.11

Pujol, M., Marty, B., Burgess, R., Turner, G., Philippot, P., 2013. Argon isotopic composition of Archaean atmosphere probes early Earth geodynamics. Nature 498, 87–90. https://doi.org/10.1038/nature12152

Rudnick, R.L., Gao, S., 2003. Composition of the Continental Crust, in: Treatise on Geochemistry. https://doi.org/10.1016/B0-08-043751-6/03016-4

Sarda, P., Staudacher, T. and Allegre, C.J., 1985. 40Ar36Ar in MORB glasses: constraints on atmosphere and mantle evolution. Earth Planet. Sci. Lett., 72(4), 357-375.

Stuart, F.M., Mark, D.F., Gandanger, P., McConville, P., 2016. Earth-atmosphere evolution based on new determination of Devonian atmosphere Ar isotopic composition. Earth Planet. Sci. Lett. https://doi.org/10.1016/j.epsl.2016.04.012

Tucker, J.M., Mukhopadhyay, S., 2014. Evidence for multiple magma ocean outgassing and atmospheric loss episodes from mantle noble gases. Earth Planet. Sci. Lett. https://doi.org/10.1016/j.epsl.2014.02.050

Williams, C.D., Mukhopadhyay, S., 2019. Capture of nebular gases during Earth's accretion is preserved in deep-mantle neon. Nature. https://doi.org/10.1038/s41586-018-0771-1